Whitmarsh, R.B., Sawyer, D.S., Klaus, A., and Masson, D.G. (Eds.), 1996
Proceedings of the Ocean Drilling Program, Scientific Results, Vol. 149

16. MAGNETOSTRATIGRAPHY OF CENOZOIC SEDIMENTS RECOVERED FROM THE IBERIA ABYSSAL PLAIN[1]

Xixi Zhao,[2] Doris Milkert,[3] Li Liu,[4] and Toshiya Kanamatsu[5]

ABSTRACT

We conducted a combined paleomagnetic and biostratigraphic study on the Cenozoic sedimentary sequences of the Iberia Abyssal Plain west of Portugal, focusing on Ocean Drilling Program Sites 897, 898, and 900. Magnetic directions at these sites were obtained by both shipboard pass-through cryogenic magnetometer measurements and onshore progressive alternating-field and thermal demagnetization experiments of more than 1000 discrete samples. Sedimentary sections of late Neogene age from Holes 897C, 898A, and 900A have recorded a pattern of magnetic polarity reversals that correlates well with the known magnetic polarity time scale for the past 5 Ma, and allows the determination of accurate sediment-accumulation rates. The polarity patterns from the Pliocene-Pleistocene turbidite sequence show that a reliable magnetostratigraphy can be established from early Pliocene to Holocene, including the Gilbert/Gauss boundary (3.58 Ma) through the Matuyama/Brunhes boundary (0.78 Ma). Below the middle Miocene angular unconformity that separates the Pliocene-Pleistocene turbidites from the Miocene and earlier strata, a reliable magnetostratigraphy could not be established because of the extremely weak magnetization of the sediments. This sudden decrease in magnetic signal corresponds in general to a large decrease in iron content and an increase in sulfate concentration, suggesting a magnetic mineral dissolution. Downhole magnetic susceptibility and intensity values provide a useful basis for correlation of this change between sites, and present a magnetic boundary among the Leg 149 sites. This magnetic boundary may be caused by the termination in supply of the terrigenous material at the end of the early Miocene and reflects the occurrence of the tectonic folding event at this time in much of western Iberia. A short sedimentary hiatus in the early Pleistocene, or a decrease in accumulation rate, was recognized at all three sites. This hiatus may represent an oceanographic event that affected a significant part of the Iberia Abyssal Plain region, such as the Arctic glaciation in Pleistocene.

INTRODUCTION

Deep-sea basins are one of the least-known sedimentary environments although they cover almost one-quarter of the Earth's surface (McKenzie, 1978). Abyssal plains within the deep-ocean basins are important because they may provide records of major tectonic events in the erosional and depositional history of a continental margin. The use of deep-sea drilling techniques to investigate the geological evolution of the ocean basins and their margins depends critically on an accurate knowledge of the geological ages of the sediments found. Without such knowledge, comparisons of contemporaneous paleoenvironment in different regions cannot be made and the recognition of important geological and tectonic events, represented by such features as sedimentary hiatuses, angular unconformities, and changes in sedimentation rates, becomes impossible. Biostratigraphy, isotope stratigraphy, and magnetostratigraphy are the three principal techniques for chronostratigraphic analysis of long, continuous sedimentary sequences. Among them, biostratigraphy is the most widely used technique for determining the relative age of deep-sea sediments, and its contribution to our current understanding of the geological evolution of ocean basins cannot be overemphasized. However, this technique does suffer certain fundamental limitations. In particular, it requires the presence of suitable conditions for the existence and preservation of ancient marine organisms, and time resolution depends upon the identification of particular assemblages of rapidly evolving species. Biostratigraphic zonations generally use the first and last appearance datums for subdividing geologic time and correlating the sedimentary section, but the relative abundances of the datums are often complicated by geographic and environmental factors, or masked in the sedimentary record by dissolution effects. This can lead to local difficulties in identifying boundaries in biostratigraphic zones and in ascribing a precise synchroneity as chronostratigraphic horizons.

Geomagnetic polarity transitions, on the other hand, are the most frequent, best-dated, and globally synchronous geophysical phenomena. From the beginning, paleomagnetic studies have been an important component of the Ocean Drilling Program (ODP). Recent advances in magnetostratigraphy, especially for the Late Cretaceous and Cenozoic which have resulted from the first decade of the ODP, have been important for the refinement of chronostratigraphic framework and have enhanced the importance of magnetostratigraphy as a correlation tool in paleogeographic studies. Although the magnetostratigraphic dating technique offers certain important advantages over the micropaleontological dating method, it is itself subject to limitations. For example, it is first necessary to demonstrate that the remanent magnetization of the sediment is stable primary magnetization acquired at, or close to, the time of deposition. Second, the pattern of magnetic reversals recorded in the particular sedimentary sequence will depend on both the reversal frequency at the time of deposition and on the sedimentation rate. In the case of slow sedimentation rates at times of high reversal frequency, certain magnetic polarity events may be too short in duration to be recorded at all, and the occurrence of sedimentary hiatuses will considerably complicate the identification of particular magnetic polarity intervals. However, if the approximate age of the sediment is known from biostratigraphic information, it should be possible to focus on a particular part of the established polarity time scale, and thus to identify specific reversals in the sedimentary sequence. The combination of magnetic and biostratigraphic studies may then allow much more precise dating than is possible from paleontological information alone.

[1]Whitmarsh, R.B., Sawyer, D.S., Klaus, A., and Masson, D.G. (Eds.), 1996. *Proc. ODP, Sci. Results,* 149: College Station, TX (Ocean Drilling Program).
[2]Institute of Tectonics, University of California, Santa Cruz, CA 95064, U.S.A. xzhao@earthsci.ucsc.edu
[3]Institute of Oceanographic Sciences, Deacon Laboratory, Wormley, Godalming, Surrey GU85UB, United Kingdom.
[4]Department of Geology, Florida State University, Tallahassee, FL 32306-3026, U.S.A.
[5]Ocean Research Institute, University of Tokyo, 1-15-1 Minamidai, Nakano-ku, Tokyo 164, Japan.

The general pattern of geomagnetic field polarity reversal during the Cenozoic and late Mesozoic is now well established (Cande and Kent, 1992). In recent years, high-precision radiometric and astronomical dating methods have become more widely available in a magnetostratigraphic context, and the absolute ages of major polarity transitions have been dated in the standard geomagnetic polarity time scale (GPST; Shackleton et al., 1990; Hilgen, 1991; Cande and Kent, 1995; Wei, 1995). However, precise correlation between the GPST and biostratigraphic zonations is still incompletely established. The only completely satisfactory means of achieving such a correlation is to undertake combined paleomagnetic and biostratigraphic studies on the same sedimentary sequences. The purpose of this paper is to present the results of such work, conducted on sedimentary cores drilled at Leg 149 sites from the Iberia Abyssal Plain. We first describe and discuss the paleomagnetic polarity patterns of the sediments recovered from Sites 897, 898, and 900, focusing on the portions that provided the most readily interpretable data. We then interpret the polarity sequence, based in conjunction with the lithostratigraphy, biostratigraphy and the newly revised geomagnetic polarity time scale (Cande and Kent, 1995; Wei, 1995), and present a magnetostratigraphy for these three sites. Finally, we use the magnetostratigraphy to estimate the sediment-accumulation rates and the times at which significant changes in these rates occurred. These estimates and between-site comparisons not only have enabled us to locate the depth of a possible magnetic dissolution in the Upper Miocene, but also led to the recognition of a significant hiatus about the Pliocene-Pleistocene boundary. Such information has importance in evaluating the recent geological evolution of the Iberia Abyssal Plain.

SITE AND GEOLOGIC SETTING

The site locations (Fig. 1) and tectonic history of the Iberia Abyssal Plain are documented in detail in the site report chapters and appropriate papers (see Sawyer, Whitmarsh, Klaus, et al., 1994) and will be only briefly summarized here.

Site 897 is situated over a north-south basement ridge that had been linked to a peridotite ridge drilled west of Galicia Bank 140 km to the north (Fig. 1). Cores were obtained from three holes that penetrated up to 694 m of Pleistocene to Early Cretaceous age sediments (Fig. 2). At Site 898, which is situated over an elongate basement high, cores were obtained from a single hole that penetrated 342 m of Pleistocene to late Oligocene age sediments. Site 899 lies within the same part of the ocean/continent transition as Site 898, and is about 20 km east of Site 897. Cores were obtained from two holes that penetrated 565 m of late Pliocene to Late Cretaceous age sediment overlying a thick series of three serpentinite breccias. The entire Pleistocene and part of the upper Pliocene are not represented in the cores recovered at Site 899. Site 900 is situated over the crest of a roughly circular basement high that on the basis of the low magnetic anomalies around it was expected to be part of the Iberia continental crust that was thinned during the Early Cretaceous rifting. Drilling and coring at this site include 749 m of Paleocene to Pleistocene contourites, turbidites, and pelagic/hemipelagic sediments (Fig. 2). Finally, Site 901 was drilled from a fault block that overlies thinned continental crust. Seven cores with very poor recovery were obtained from this site, with ages ranging from Pliocene to Late Jurassic.

A major characteristic of the seismic-reflection profiles obtained off much of western Iberia is an angular unconformity caused by onlap of mainly Pliocene-Pleistocene turbidites onto gently folded middle Miocene and earlier strata. The folding is the result of a northwest-southeast compressional phase in the Beti mountains of southern Spain (Mauffret et al., 1989). This regional unconformity was recognized at all sites and dated as middle Miocene based on preliminary shipboard biostratigraphical data. The end of the hiatus was more variable and probably depended on the amount of uplift at each site (Shipboard Scientific Party, 1994a-c).

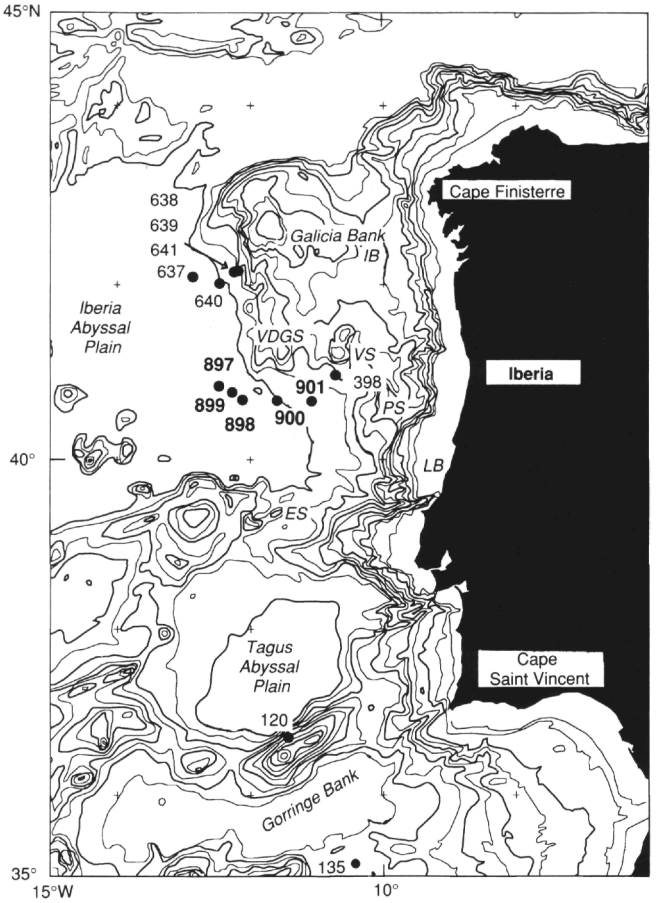

Figure 1. Regional bathymetric chart of the western Iberia Margin (contours in 500-m intervals, 1000-m contours in bold). Smaller numbers refer to previous DSDP/ODP sites; larger numbers refer to sites drilled during Leg 149. IB = Interior Basin, VDGS = Vasco da Gama Seamount, VS = Vigo Seamount, PS = Porto Seamount, LB = Lusitanian Basin, ES = Estremadura Spur.

LABORATORY AND ANALYTICAL METHODS

Paleomagnetic Sampling

During Leg 149, more than 1000 discrete paleomagnetic samples were taken for shipboard and shore-based magnetostratigraphic and rock magnetic studies. In the case of soft unconsolidated sediments, paleomagnetic samples were taken by pushing nonmagnetic cubes into the split working halves. In order to reduce the deformation/disturbance of the sediment, the core was carefully cut using a thin stainless-steel spatula before pressing the plastic sampling boxes into the sediment.

In lithified sediments, 2.5-cm cylindrical samples were drilled from the core sections using a water-cooled nonmagnetic drill bit attached to the standard drill press, or cube-shaped samples were cut by diamond saw. In all cases the uphole direction was carefully recorded on the sample by means of an orientation arrow before removal from the core section, and only sediments showing no visible signs of deformation were sampled. All samples were kept in a relatively cold temperature and low-field environment (field-free room) to inhibit water loss and prevent viscous remanence acquisition.

Magnetic Measurement Procedure

The paleomagnetic data presented in this paper are of two different types: those obtained using the shipboard pass-through cryogenic

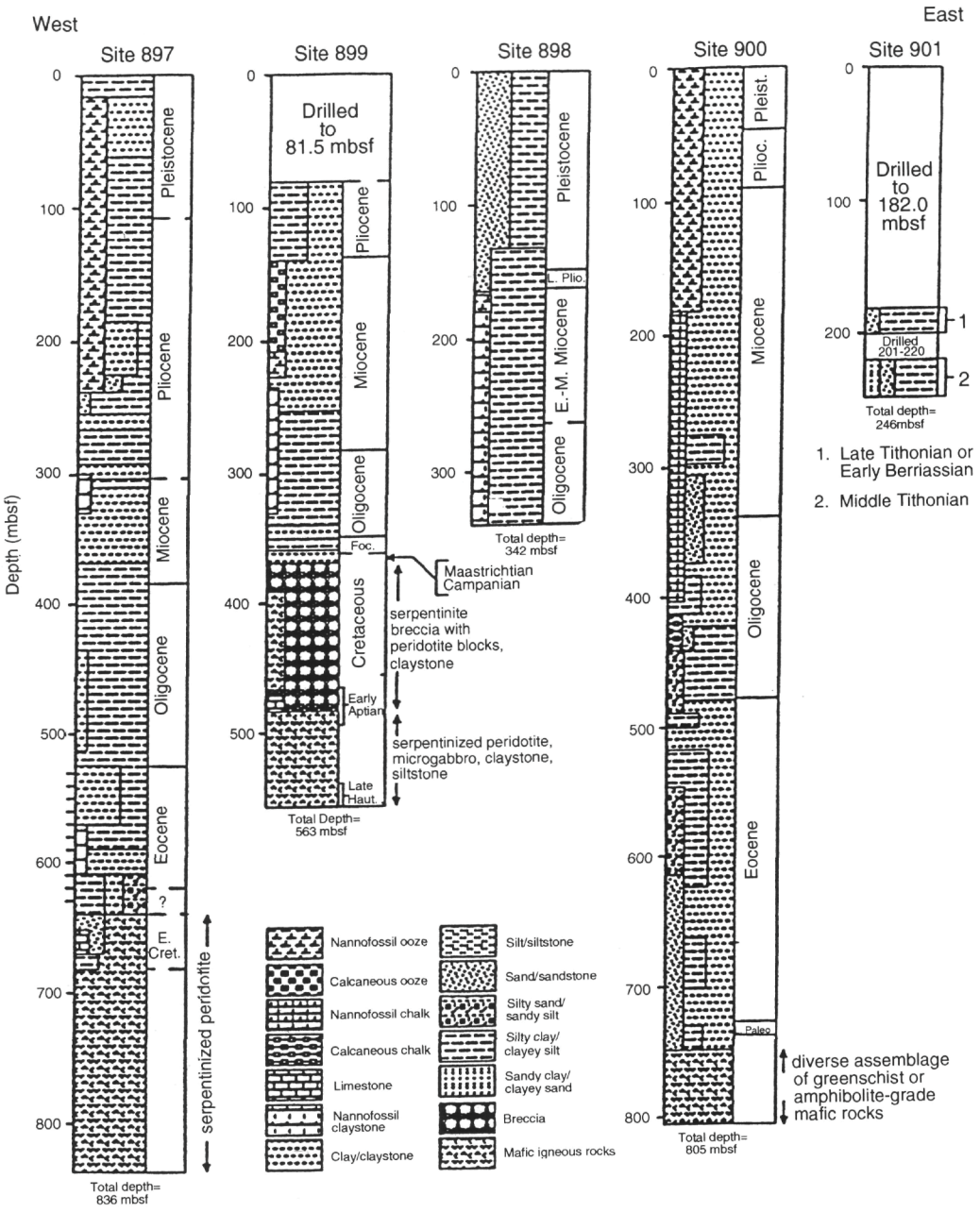

Figure 2. Summary lithological columns from the five sites drilled during Leg 149 in the Iberia Abyssal Plain.

magnetometer and those derived from onshore analysis of discrete samples. In the shipboard pass-through system, magnetic measurements were performed by passing continuous achieve-half core sections through a 2G cryogenic magnetometer, and were taken at intervals of either 5 or 10 cm along the core, and after alternating field (AF) demagnetization at 10 and 15 mT. Magnetic measurement of discrete samples in the shore-based studies was performed with a 2G cryogenic magnetometer and a Schonstedt spinner magnetometer housed in a field-free room in the paleomagnetic laboratory at the University of California at Santa Cruz (UCSC). A few samples were also measured at the Ocean Research Institute, University of Tokyo. Both standard thermal and AF demagnetization experiments were done using Schonstedt equipment to evaluate the directional stability and coercivity/unblocking temperature spectra of each sample.

In order to assess the reliability of the polarity determinations, a vector diagram was used for each sample to identify the magnetic components of magnetization that were present. Magnetic components were determined by fitting least-squares lines to segments of the vector demagnetization plots or "the principal component analysis" (Zijderveld, 1967; Kirschvink, 1980) that were linear in three-dimensional space. Results from samples exhibiting no stable directional end point were discarded on the grounds that they were either unstable or carried a complex remanence that could not be satisfactorily resolved by available laboratory techniques.

Because of the rotary technique used for drilling Leg 149 cores, relative rotation commonly occurs between different segments of sediment within the core, and this will cause apparent changes in the declination of stable remanent magnetization. Consequently, in this study the magnetic polarity has been assigned on the basis of the inclination of the stable remanent magnetization alone as is commonly done in ODP work. Because all sites are situated at moderate latitudes in the Northern Hemisphere, positive (downward directed) inclinations are taken to signify a normal polarity, and negative (upward directed) inclination reversed polarity. In this study, we adhere to the

chronostratigraphic nomenclature and geochronology of Cande and Kent (1995) and Wei (1995), and use their tables as the GPST. We correlate polarity zones with the GPST in the manner that appears most consistent with both the magnetic and biostratigraphic data. In naming the various polarity intervals, we use the familiar proper names for the Pliocene-Pleistocene magnetic chrons (Brunhes, Matuyama, Gauss, and Gilbert) and subchrons (e.g., Jaramillo and Olduvai).

MAGNETIC RESULTS

General View

Continuous and undisturbed Cenozoic sections of sufficient length to allow the identification of geologically useful magnetic polarity sequences were obtained from Sites 897, 898, and 900 but not from Sites 899 and 901. Therefore, Sites 899 and 901 will not be considered any further in this paper.

Within the three sites for which magnetostratigraphy can be constructed, there are considerable variations in demagnetization behavior among the various lithologies, as be described in detail below, but the most common features can be summarized as follows: a pervasive remagnetization imparted by the coring process is common as noted during previous legs (e.g., Zhao et al., 1994). This remagnetization is characterized by natural remanent magnetization (NRM) inclinations that are strongly biased toward the vertical value (+90°) in many cores. This remagnetization most severely affected the external portions of the cores (presumably because the outside of the core is physically closer to the magnetized core barrel). When present, this drilling-induced component generally shows a steep downward direction and can be removed at the initial stages of demagnetization. As shown in Figure 3, the NRM inclinations observed from Section 149-897C-61R-1 are biased toward steep positive values, indicating the presence of drilling-induced remagnetization. Upon demagnetization to 15 mT, a shift toward a negative inclination and a significant decrease in intensity were observed. The reversed polarity of magnetization was also confirmed by progressive AF demagnetization on three discrete samples from this section (squares in Fig. 3). Because the maximum level of AF demagnetization on the ship's cryogenic magnetometer could not always remove these overprints, the pass-through measurements generally show a more intense remagnetization than do the discrete sample measurements. Therefore, the majority of the paleomagnetic results presented in this paper were obtained from extensive shore-based measurements on discrete samples carried out in the "field-free" paleomagnetic laboratory at UCSC.

Whenever possible, demagnetization was continued until it was considered that an unambiguous and reliable determination of the polarity of the stable component of magnetization had been achieved. Figure 4 illustrates the demagnetization behavior of several samples from nannofossil clay and ooze. AF demagnetization of Sample 149-900A-14R-1, 15-17 cm, demonstrates the removal of a normal component of magnetization close to the present geomagnetic field inclination and the isolation of a more stable reverse component that is univectorially decaying toward the origin of the vector plots. Sample 149-900A-10R-2, 35-37 cm, on the other hand, shows a reversed secondary component that was removed before the more stable normal polarity of characteristic remanent magnetization (ChRM). Examples of thermal demagnetization are also illustrated in Figure 4 (Samples 149-900A-49R-2, 60-62 cm, and 149-900A-49R-7, 26-28 cm). A secondary magnetic component of magnetization was removed at low temperatures (300°C) and the ChRM component with higher unblocking temperatures could be identified. These demagnetization behaviors are typical of the majority of samples from all three sites. The demagnetization of some discrete samples also shows antipodal relative declinations within the same piece of core section. An example is given by two samples from Core 149-900A-10R (Fig. 5). It is significant that both samples were taken from the same core section, and after demagnetization at 40 mT the reversal indicated by the difference in polarity of inclination is confirmed by the nearly 180° in declination. This positive "antipodal test" is perhaps the most compelling argument for isolating the primary ChRM, although this test is not sufficient by itself. The inclination values of ChRM are moderately downward or upward which are consistent with the expected inclination for these sites. This information may imply that the ChRM of these sediments is free of the secondary component of magnetization and represents the primary magnetization when these sediments were deposited. Although the shipboard alternating field demagnetization of Pliocene-Pleistocene sediments at Sites 897, 898, and 900 revealed initial polarity patterns (see "Paleomagnetism" section, Shipboard Scientific Party, 1994a-c), the subsequent shore-based thermal and detailed AF demagnetization were able to resolve a high-coercivity/unblocking temperature component, improved the quality of the magnetostratigraphy.

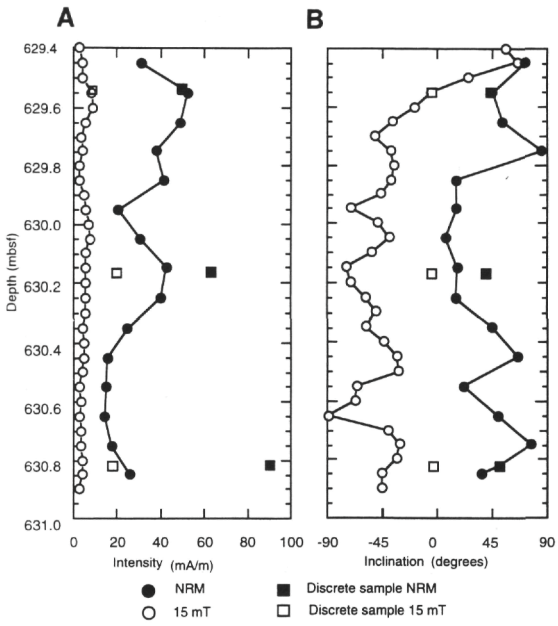

Figure 3. Remanent magnetization before and after 15-mT AF demagnetization as a function of sub-bottom depth. Intensities (**A**) and inclinations (**B**) of archive halves and discrete samples from Section 149-897C-61R-1 are shown. The NRM inclinations are biased toward high positive inclinations, suggesting that drilling-induced magnetization is present. AF demagnetization to 15 mT can effectively remove this drilling-induced magnetization, as indicated by changes in inclination and intensity.

Site 897 (Hole 897C)

Sampling and Stability Tests

A total of 330 oriented paleomagnetic samples (6-cm^3 plastic cubes or 10-cm^3 minicores) was collected from Cenozoic sediments at this hole, spaced at least at one sample per section. Each of these 330 samples was subjected to progressive AF or thermal demagnetization to verify the magnetostratigraphic results from the cryogenic magnetometer and to understand the magnetic behavior of the sediments during stepwise demagnetization. Figure 6 illustrates the response to AF demagnetization of two samples from nannofossil chalk oozes. The high stability showed by normally magnetized Sample 149-897C-4R-1, 34-36 cm, and reversely magnetized Sample 149-897C-11R-6, 37-39 cm, is characteristic of a high proportion of the samples from Hole 897C. These samples maintain an inclination close to the theoretically predicted value for the latitude of this site, indicating they may represent the primary ChRM.

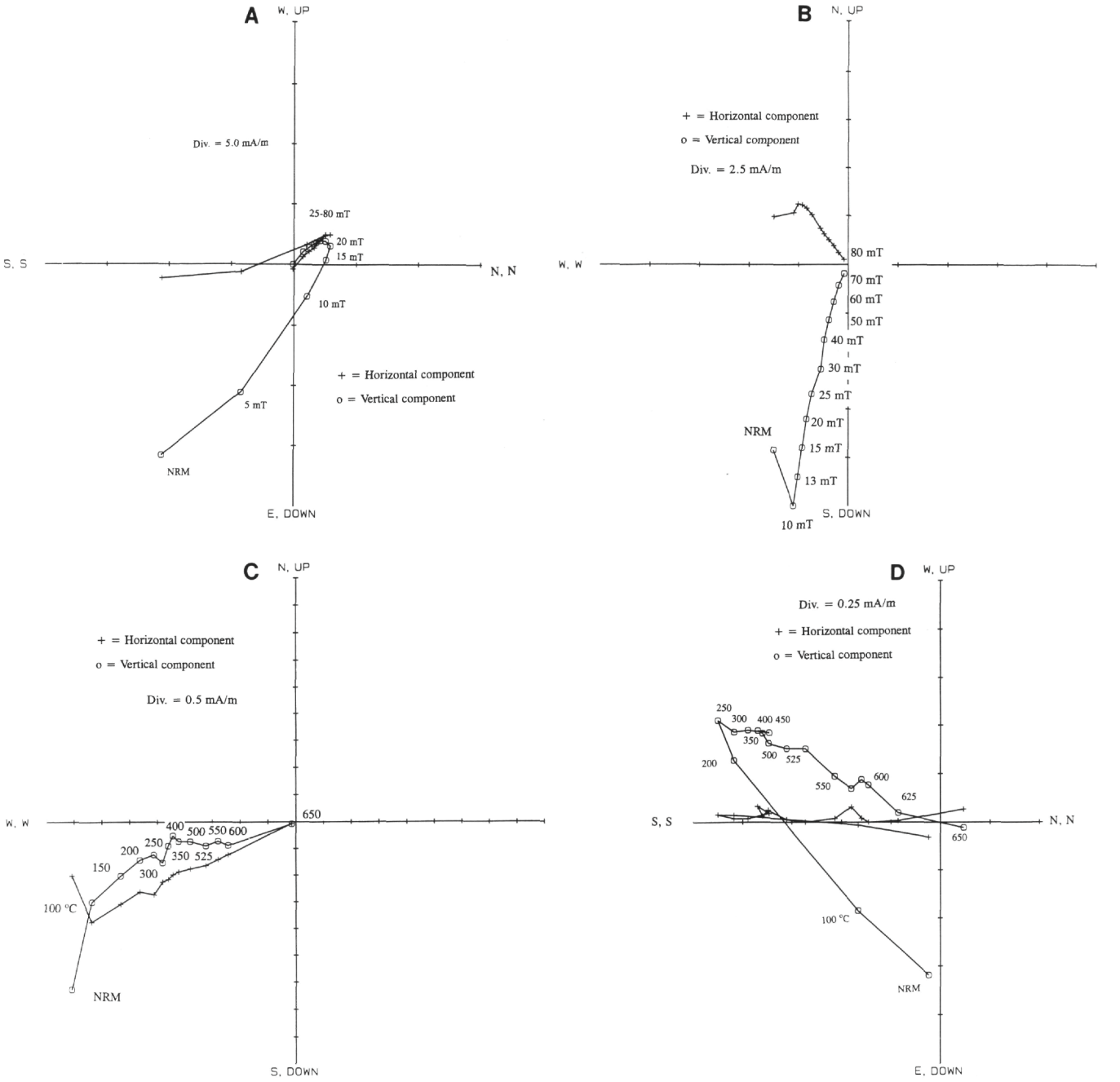

Figure 4. Representative vector end-point diagrams showing the results of thermal and AF demagnetization for samples of nannofossil clay and nannofossil ooze. Crosses and circles represent the projection of the magnetization vector end point on the horizontal and vertical planes, respectively. **A.** Sample 149-900A-14R-1, 15-17 cm, shows the removal of a normal component of magnetization close to the present geomagnetic field inclination and isolation of a more stable reverse component that is univectorially decaying toward the origin of the vector plot. **B.** Sample 149-900A-10R-2, 35-37 cm, exhibits a reversed secondary component that was removed before the more stable normal polarity of characteristic remanent magnetization (ChRM). **C.** and **D.** Demonstrations of the demagnetization behavior of samples during thermal demagnetization. Sample 149-900A-49R-2, 60-62 cm, and Sample 149-900A-49R-7, 26-28 cm, show normal and reversed polarity of ChRM, respectively.

Magnetic Polarity Record for Hole 897C

As shown in Table 1 and Figure 7, a number of clearly defined magnetic reversals may be discerned on the basis of changes in sign of the inclinations of the cores from Hole 897C. Without exception, each of the major polarity zones is defined by several samples of the same polarity. On the basis of micropaleontological studies, the uppermost 180 m of sediment at Site 897 is known to be of Pleistocene age (see Liu and Mariono, this volume; Gervais, this volume). Therefore, the normal polarity of Cores 149-897C-1R through 7R suggests that these sediments were deposited during the Brunhes chron (i.e., age <0.78 Ma), which agrees well with the biostratigraphic age markers (see Liu and Mariono, this volume; Gervais, this volume). The first evidence for a reversed magnetization occurs at 118.93 meters below sea floor (mbsf) in Core 149-897C-8R, which corresponds to the Brunhes/Matuyama chron boundary (0.78 Ma) and biostratigraphic Zones NN19h andN23. Samples between 128.72 and 137.40 mbsf show normal polarity, indicating the Jaramillo subchron (0.99-

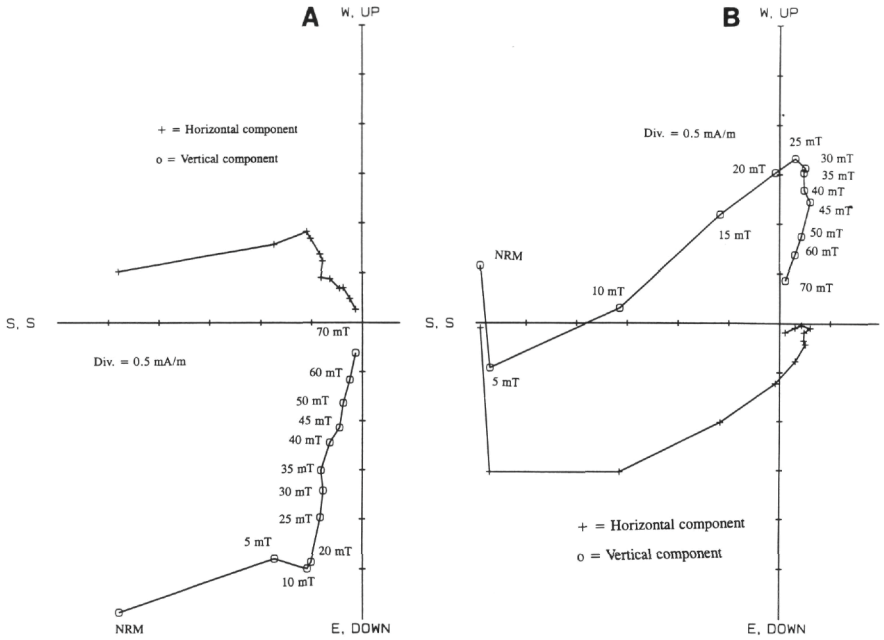

Figure 5. Representative vector end-point diagrams showing the results of alternating field demagnetization for samples from Core 149-900A-4R. **A.** Sample 149-900A- 10R-4, 7-9 cm. **B.** Sample 149-900A-10R-4, 139-141 cm. Crosses and circles represent the projection of the magnetization vector end point on the horizontal and vertical planes, respectively. Note that both samples were taken from same piece of continuous core section, and, after demagnetization at 40 mT, the reversal indicated by the difference in polarity of inclination is confirmed by the nearly 180° in declination, adding confidence to the polarity determination.

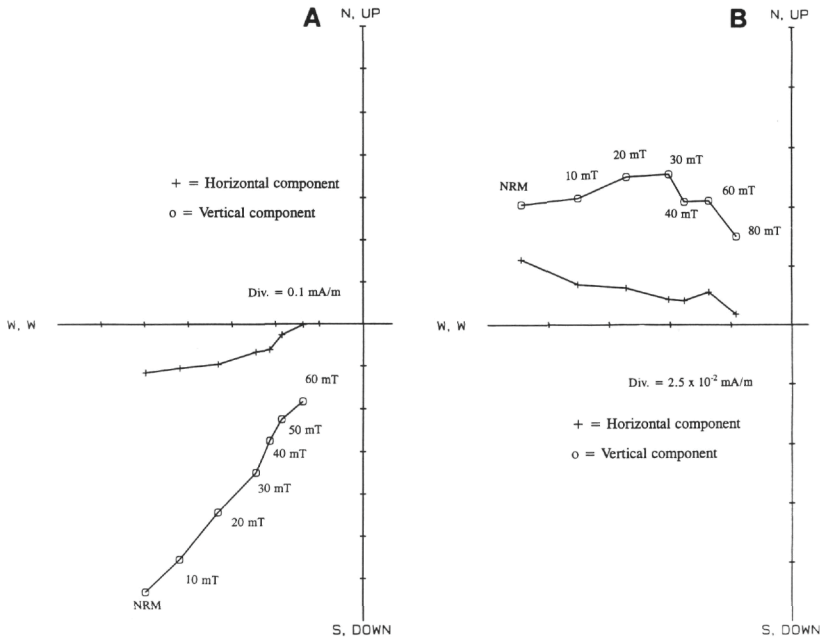

Figure 6. Representative vector end-point diagrams showing the results of AF demagnetization for samples from Site 897. Crosses and circles represent the projection of the magnetization vector end point on the horizontal and vertical planes, respectively. Sample 149-897C-4R-1, 34-36 cm (**A**), shows normal polarity and 149-897C-11R-6, 37-39 cm (**B**), shows reversed polarity of ChRM.

1.07 Ma). Biostratigraphic Zone NN19g (0.88-1.07 Ma) is also placed in this depth interval. Below this depth, the dominantly reversed polarity correlates well with the Matuyama reversed polarity chron. This dominantly reversed polarity sequence extends to a depth of 292.8 mbsf. Biostratigraphic data suggest that sediments below a depth of 292.4 mbsf (Core 149-897C-26R, 93-94 cm) may be of early Pliocene age. This information is in good agreement with the paleomagnetic observations, and suggests that the shift of polarity from reversed to normal at about 292 mbsf should correspond to the Matuyama/Gauss boundary (2.58 Ma). Within the sequence assigned to the Matuyama reversed chron, two apparently separate thin normal polarity zones are present at depths of 198.79 to 207.33 mbsf and 234.14 to 235.66 mbsf, respectively. The upper of these polarity zones is well defined on the basis of seven separate samples and appears to correspond well with the position of the Olduvai subchron (1.77-1.95 Ma). Key nannofossil and planktonic foraminiferal markers around this depth also suggest that the sediments span the Pliocene and Pleistocene boundary (NN19a and N22), which is in

Table 1. Paleomagnetic results from Hole 897C used to determine magnetostratigraphy at Site 897.

Core, section, interval (cm)	Depth (mbsf)	NRM intensity (mA/m)	AF demag step (mT)	Inclination (°)	Polarity
149-897C-					
1R-1, 102–104	50.92	0.87	50	55.1	N
1R-2, 61–64	52.01	0.05	20	41.3	N
2R-1, 88–90	60.78	0.295	70	33	N
2R-1, 121–123	61.11	0.88	80	39.2	N
2R-2, 7–9	61.47	7.41	50	61.6	N
3R-1, 83–85	70.43	2.91	70	57.7	N
4R-1, 34–36	79.54	0.812	60	50.7	N
5R-1, 27–30	89.17	1.98	85	33.5	N
5R-2, 67–69	91.07	4.13	60	41.8	N
6R-1, 27–30	98.77	1.19	60	34.2	N
6R-1, 58–61	99.08	1.05	60	46.9	N
6R-2, 96–98	101.88	21.67	50	49.1	N
7R-1, 54–57	108.7	1.36	50	28.7	N
7R-1, 62–65	108.8	0.29	50	42.2	N
8R-1, 103–105	118.9	6.77	99	–50.3	R
8R-1, 123–125	119.1	4.75	99	–46.7	R
8R-2, 81–83	120.2	0.09	80	–52.8	R
8R-2, 110–112	120.5	0.05	80	–55.2	R
8R-3, 20–22	121.1	0.08	80	–50.2	R
8R-3, 79–81	121.7	0.08	80	–52.6	R
9R-2, 19–21	128.7	0.07	20	38.6	N
9R-2, 53–55	129.1	0.03	70	36.8	N
10R-1, 20–22	137.4	1.93	80	–40.5	R
10R-1, 62–64	137.8	0.02	50	–56.7	R
10R-1, 121–123	138.4	0.03	40	–55	R
11R-2, 28–30	147.4	3.2	70	–53.3	R
11R-2, 31–33	147.4	0.89	60	–51.8	R
11R-3, 52–54	148.8	0.32	60	–62.1	R
11R-3, 125–127	149.6	0.65	60	–63.6	R
11R-4, 14–16	150	1.23	60	–64.1	R
11R-4, 66–68	150.5	0.08	60	–53.6	R
12R-6, 31–33	164.4	0.49	40	–55.8	R
12R-6, 37–39	164.5	0.13	99	–57.9	R
14R-1, 44–46	176.2	0.34	60	–49.8	R
14R-1, 69–71	176.5	0.52	70	–48.7	R
14R-2, 6–8	177.4	0.06	70	–72.8	R
14R-2, 15–17	177.5	0.19	80	–49.3	R
14R-2, 29–31	177.6	0.24	60	–47.4	R
14R-3, 6–8	178.9	0.11	60	–24.6	R
14R-3, 18–20	179	0.02	30	–9.4	R
14R-3, 123–125	180	0.03	30	–51.6	R
14R-4, 3–5	180.3	0.36	30	–21.4	R
14R-4, 70–72	181	0.38	30	–40.2	R
14R-4, 110–112	181.4	0.02	30	–52.9	R
15R-1, 26–29	185.7	3.76	60	–13.2	R
15R-1, 134–136	186.7	0.09	50	–53.5	R
15R-2, 11–13	187	0.08	40	–52.8	R
15R-2, 85–87	187.8	0.18	40	–59.1	R
15R-3, 71–74	189.1	2.57	60	–51.4	R
15R-3, 121–123	189.6	5.69	80	–39.5	R
15R-4, 24–27	190.1	2.67	50	–60	R
16R-1, 36–38	195.5	0.07	80	–73.5	R
16R-1, 57–59	195.7	0.09	80	–66	R
16R-2, 57–59	197.2	0.09	80	–38.3	R
16R-2, 93–95	197.5	0.09	80	–65.7	R
16R-3, 10–12	198.2	0.07	60	30.6	N
16R–3, 69–71	198.8	0.48	50	52.5	N
16R-4, 35–37	200	0.63	40	44.8	N
17R–1, 20–22	204.9	0.02	30	20.9	N
17R-1, 42–44	205.1	0.22	40	11.9	N
17R-1, 132–134	206	0.02	20	46.1	N
17R-2, 24–26	206.4	0.07	40	48.8	N
17R-2, 113–115	207.3	0.03	40	–12.5	R
18R-1, 33–35	214.7	0.54	60	–47.7	R
18R-1, 38–40	214.8	0.07	50	–35.8	R
19R-1, 36–38	224.5	25.1	80	–52.6	R
19R-2, 38–40	226	20.5	80	–59.5	R
19R-2, 74–76	226.34	8.9	60	–60	R
19R-2, 99–101	226.6	16.3	60	–53.7	R
19R-3, 73–75	227.8	9.57	80	–58.4	R
19R-3, 114–116	228.2	1.32	70	–57.5	R
19R-4, 52–54	229.1	0.17	60	–71.8	R
19R-4, 68–70	229.3	0.07	60	–59.4	R
20R-1, 34–36	234.1	0.04	30	–55.9	R
20R-1, 51–53	234.3	0.04	30	63.5	N
20R-1, 93–95	234.7	0.1	45	46.4	N
20R-2, 36–38	235.7	0.11	60	–45.5	R
20R-2, 45–47	235.8	0.04	40	–65	R
20R-2, 69–71	236	3.5	80	–56.1	R
20R-2, 90–92	236.2	2.96	60	–65.8	R
21R-1, 18–21	243.6	2.44	60	–57.8	R
21R-1, 69–71	244.1	3.88	60	–52.9	R
21R-1, 109–111	244.5	1.18	50	–49.8	R
22R-1, 87–89	253.9	0.65	70	–62.8	R
22R-1, 100–102	254	1.81	60	–54.8	R
22R-1, 120–122	254.2	0.19	60	–63.2	R
22R-2, 107–109	255.6	0.56	40	–56.2	R
22R-2, 140–142	255.9	5.15	50	–57.4	R
22R-5, 11–13	259.1	4.49	70	–63.9	R
22R-5, 26–28	259.3	6.08	70	–47.2	R
23R-1, 63–65	263.3	0.13	60	–55.1	R
23R-1, 132–134	264	0.15	60	–5.4	R
23R-2, 39–41	264.6	0.04	30	–41.4	R
23R-2, 41–43	264.6	0.05	50	–31.6	R
23R-3, 45–47	266.2	0.06	60	–53.2	R
23R-3, 47–49	266.2	0.08	40	–20.4	R
24R-1, 90–92	273.2	2.15	50	–65.6	R
24R-1, 124–126	273.5	2.64	50	–73.4	R
24R-2, 20–22	274	1.7	50	–72.8	R
24R-2, 20–24	274.02	2.7	50	–31.5	R
24R-2, 36–38	274.2	0.86	65	–67.6	R
25R-1, 21–23	282.2	6.88	50	–56.4	R
25R-2, 4–6	283.4	0.46	40	–63	R
25R-2, 49–51	283.8	0.21	40	–44.6	R
26R-1, 138–140	292.9	6.26	15	–14.4	R
26R-2, 91–93	293.9	3.89	15	–59.7	R
26R-2, 120–122	294.2	0.34	15	53.9	N
28R–1, 81–83	311.7	5.78	15	41.7	N
28R-1, 90–92	311.8	3.8	15	55.3	N
28R–2, 91–93	313.3	3.93	15	–30.1	R?
28R-2, 100–102	313.4	2.88	15	–31.2	R?
28R-2, 124–126	313.6	6.7	15	38.3	N
28R–3, 32–34	314.2	2.22	15	–42.8	R
28R-3, 42–44	314.3	3.66	15	–27.1	R
28R-4, 100–102	316.4	2.15	15	0.1	R?
29R-1, 27–29	320.79	4.92	15	26.7	N
29R-1, 81–83	321.31	7.27	15	–17.6	R
29R-2, 116–118	323.16	2.67	15	31.2	N
29R-3, 115–117	324.66	2.91	15	21.1	N
29R-4, 37–39	325.38	3.51	15	0.7	N?
29R-5, 75–77	327.26	1.63	15	22.9	N
29R-6, 43–45	328.44	1.12	15	12.2	N
30R-1, 56–58	330.76	3.65	15	4.1	N?
30R-2, 110–112	332.8	0.14	15	60.9	N
30R-3, 14–16	333.34	0.91	15	0.3	N?
30R-3, 75–77	333.95	0.5	25	10.6	N?

Notes: AF demag step = highest peak field applied during progressive alternating field demagnetization, inclination = stable inclination after demagnetization, N/R = normal/reversed polarity.

good agreement with the paleomagnetic data. The underlying thin normal polarity zone at 234.14 mbsf is based on only two samples with a high magnetic stability, but it is quite possible that they represent the short Reunion subchron (2.14-2.15 Ma). Below the Matuyama/Gauss boundary, there is a dominantly normal polarity sequence, extending down at least to 333.95 mbsf (Table 1). This dominantly normal polarity sequence should correspond to the Gauss normal chron. Unfortunately, sediments below 333.95 mbsf are too weakly magnetized to be measured reliably. The NRM intensity is essentially the same order as the noise level of the cryogenic magnetometer and the sample holder. Consequently, this weak magnetization prevents us from constructing the magnetostratigraphy below this depth.

The paleomagnetic and biostratigraphic datums are summarized in Table 2, and the main features of the magnetostratigraphic interpretation along with the inferred biostratigraphic zones at Site 897 are presented in Figure 7. It is clear from Table 2 and Figure 7 that the paleomagnetic and paleontological age determinations for the Pleistocene to early Pliocene sequence at Hole 897C are compatible with each other, but the resolution of the paleomagnetic data is significantly greater. This allows a more precise determination of sediment-accumulation rates and a better definition of the times at which significant changes in the sedimentation rate occurred.

Paleomagnetically Determined Sedimentation Rates for Hole 897C

The Pleistocene and Pliocene sediments cored at Hole 897C have yielded a detailed magnetic polarity stratigraphy, from which relatively precise sedimentation rates can be calculated. The Brunhes/Matuyama (0.78 Ma), Jaramillo (0.99-1.07 Ma), Olduvai (1.77-1.95 Ma), and Matuyama/Gauss (2.58 Ma) chrons are well determined at depths of 118.9, 128.7-137.4, 198.2-207.3, and 292.88 mbsf, respectively.

One thin normal polarity zone at 234.1 mbsf is based on two samples but may possibly represent the Reunion subchron (2.14-2.15 Ma).

With these calibration points, the Site 897 magnetic polarity sequence is plotted against the GPTS in Figure 8. The correlation allows the determination of relatively precise sedimentation-accumulation rate values and the assignment of "absolute" ages to the biostratigraphic zonal boundaries identified at Hole 897C. The lower Pliocene to Holocene sediment-accumulation rates at Site 897C exhibit alternating high and low rates. Sedimentation rates for the late Pliocene (50.7 m/Ma) and early Pleistocene (90.3 m/Ma) show markedly reduced deposition, compared to the relative high accumulation rates during the lower Pliocene interval (135.8 m/Ma) and the upper Pleistocene to Holocene (152.4 m/Ma). Based on the correlation shown in Figure 8, a mean sedimentation accumulation rate of 92.3 m/Ma is derived for most of the Pleistocene-Pliocene. Furthermore, if the identification of the Olduvai subchron is correct, a short hiatus, or a decrease in accumulation rate, is inferred within the interval 1.77 to 1.95 Ma. It is worth pointing out that it was the paleomagnetic data that suggest the existence of a hiatus around the Pleistocene and Pliocene boundary, which could not have been identified from the available paleontological information alone.

Site 898 (Hole 898A)

Paleomagnetic Stability Test and General Polarity Sequences for Site 898

At Site 898, multiple samples were taken from each 1.5 m core section recovered, yielding a total of 266 samples. As with Hole 897C, all samples were separately subjected to progressive AF demagnetization, although only 154 samples were used to determine the magnetostratigraphy (Table 3). In addition, the entire Section 149-898A-12H-2 was specially chosen as a U-channel sample (105.70-107.20 mbsf in Table 3), which provides a unique opportunity to study a geomagnetic polarity transition in an abyssal plain setting.

The whole-core pass-through measurements from cores recovered with the advanced piston corer (APC) at Site 898 were of high quality and agree well with the discrete sample data. The mean inclination value is very close to the expected inclination (59.7°) at the site from the Pleistocene to present. The magnetic behavior for Cores 149-898A-1H through 14H is very straightforward. After removal of a "soft" overprint component of magnetization, a well-established demagnetization stable end point is defined by a linear trend through the origin of the vector plot (Fig. 9). The stable components of remanent magnetization for Cores 149-898A-1H through 3H are all of normal polarity. Biostratigraphic ages in these cores range from 0.3 to 0.8 Ma (see Sawyer, Whitmarsh, Klaus, et al., 1994, p. 122). Thus, in conjunction with the biostratigraphic data, we can assign these cores to the Brunhes chron (<0.78 Ma).

The first evidence for a polarity reversal was found in Core 149-898A-4H at a depth of 29.06 mbsf. This is shown by both discrete sample measurement and by the whole-core pass-through measurement with changes of about 180° in declination between the normal and reversed intervals (see "Paleomagnetism" section, Shipboard Scientific Party, 1994b). Thus, this magnetic polarity shift (from normal to reversed) represents the Brunhes/Matuyama boundary (0.78 Ma). The next distinctive polarity shift (from reversed to normal) occurs in Core 149-898A-11H at 101.74 mbsf and is well recorded in the U-channel Sample 149-898A-12H-2 (see Table 3 and Fig. 10). According to the sequence of magnetic polarity zones, this polarity shift may represent the onset of Jaramillo subchron (0.99-1.07 Ma). However, biostratigraphic data suggest that sediments below 95.75 mbsf may be of middle Pleistocene age (NN19d, see Liu and Mariono, this volume) and this polarity shift should correspond to the Cobb Mountain subchron at about 1.1 Ma (Mankinen et al., 1978; Mankinen and Grommé, 1982; Clement and Kent, 1987; Spell and McDougall, 1992). As the age of the Cobb Mountain subchron is estimated to be 1100±20 ka (Mankinen and Grommé, 1982; Spell and McDougall, 1992), this information suggests that sediments from 101.74 to 106.44 mbsf were deposited in less than 30 ka and implies an abruptly high sedimentation rate (157 m/Ma) during this interval compared to those for the rest of Pleistocene. In view of this apparently anomalous sedimentation rate, which is not observed in other Leg 149 sites, and the fact that the age difference between the Jaramillo and Cobb Mountain is very small (0.02 Ma), we prefer to adhere to the sequence of magnetic polarity zones and correlate this polarity change to the Jaramillo subchron.

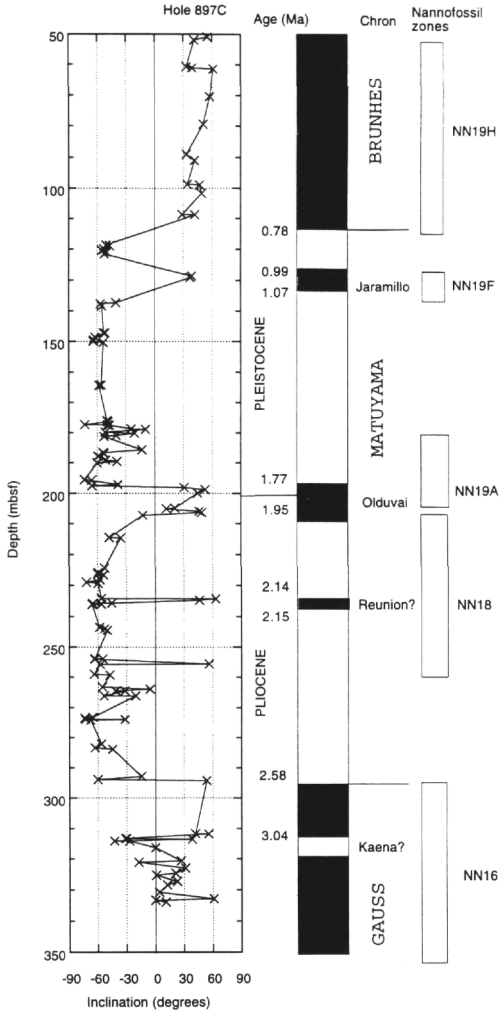

Figure 7. Downhole variation of stable magnetic inclination, inferred polarity, and biostratigraphic zones for Cenozoic sediments at Site 897. Normal polarity is indicated by black areas; reversed polarity is indicated by white areas.

Between 106.46 and 163.18 mbsf, progressive demagnetization revealed only reversed magnetization from cores recovered in this interval except a less well defined normal polarity interval at (143.85-161.82 mbsf, see Fig. 10). The observed normal polarity is in excellent agreement with the biostratigraphic age estimate (Nannofossil event NN19a, see Table 4) which corresponds to a period of expected normal polarity. Therefore, this normal polarity interval may be correlated to the Olduvai subchron. The sedimentary hiatus below 163.18 mbsf (Core 149-898A-18X) introduces a gap in the magnetostratigraphic record and complicates the identification of particular polarity chrons. However, magnetic measurements reveal that a shift of polarity from reversed to normal occurs at a depth of 197.03 mbsf (Fig. 10). Below this depth, the inclinations are dominantly normal

Table 2. Paleomagnetic and biostratigraphic datums at Site 897.

Magnetic datum (Chron or subchron)	Biostratigraphic datums (N, F)	Age (Ma)		Depth range (mbsf)	
		(magnetism)	(biostratigraphy)	(magnetism)	(biostratigraphy)
Brunhes/Matuyama	NN19h, N23	0.78	0.48–0.83	108.2	50.35–109.26
Jaramillo	NN19f	0.99–1.07	0.89–1.06	128.72–137.4	127.5–137.20
Olduvai	NN19a, N22	1.77–1.95	1.66–1.91	198.20–207.33	181.18–207.17
Reunion?	NN18	2.14–2.15	1.95–2.36	234.14–235.66	207.87–263.83
Matuyama/Gauss	NN16	2.58		292.88	292.43

Notes: N = nannofossil, F = foraminiferal datums.

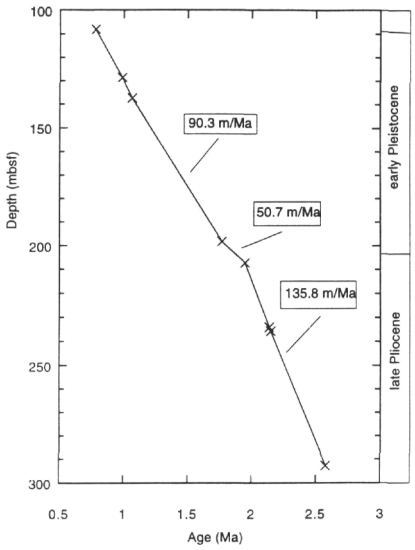

Figure 8. Depth vs. age curve for Hole 897C. The paleomagnetic data points are listed in Table 2. Note the short hiatus, or a decrease in accumulation rate, inferred within the interval 1.77 to 1.95 Ma.

between 197.03 to 206.86 mbsf, suggesting that this interval may correspond to a period of predominantly normal polarity. On the basis of foraminiferal assemblages, this interval is placed at the N7/N6 boundary. Thus, the shift of polarity from reversed to normal found at 197.03 mbsf in Core 149-898A-22X might correspond to Chron C5D (17.31-17.65 Ma). Below a depth of 209.73 to 338.5 mbsf, NRM intensities for Cores 149-898A-23X through 36X are very weak and the data are highly scattered. Although magnetic measurements also suggest several polarity reversals were recorded in these cores, these polarity signals may not be reliable because of the weak magnetization of most of the sediments. The magnetostratigraphy and biostratigraphic zones are presented in Figure 10.

Paleomagnetically Determined Sedimentation Rates for Hole 898A

Table 4 summarizes the paleomagnetic and biostratigraphic datums at Hole 898A. Similar to the reversal patterns found in Site 897, the Pleistocene and Pliocene sediments cored at Hole 898A have preserved records for (1) Brunhes/Matuyama (0.78 Ma), (2) Jaramillo (0.99-1.07 Ma), and (3) Olduvai (1.77-1.95 Ma) at depths of 29.06, 101.74-106.44, and 143.85-161.82 mbsf, respectively. From this polarity stratigraphy relatively precise sedimentation rates can be calculated. The paleomagnetic suggested mean sedimentation rates at Site 898 for the age interval 0.78 to 1.77 Ma is 115.9 m/Ma, and slightly lower (99.8 m/Ma) for a period of 1.77-1.95 Ma (Fig. 11). These estimates are comparable to those of at Site 897 (Fig. 8) and also to those of estimated from turbidite study (Milkert and Weaver, this volume). Rates could not be calculated for the sediments below 163.18 mbsf because of the hiatus and the absence of reliable chronostratigraphic event. It is significant to note that the short hiatus at about the Pleistocene/Pliocene boundary is again inferred at the paleomagnetic records of Site 898. The geological implication is discussed in a later section.

Site 900 (Hole 900A)

Magnetic Properties and Stability Tests

A total of 521 discrete samples was collected from cores at Hole 900A for shore-based measurements. A U-channel sample was also taken from Core 149-900A-10H for a detailed polarity transition study. The quality of paleomagnetic data from Site 900 depends strongly on the lithology of the recovered material; thus, the discussion here of magnetic properties at Site 900 is organized on the basis of lithology. Recovered materials from Cores 149-900A-1R to 4R are mud-dominated turbidites. These cores were too mechanically disturbed by drilling to allow meaningful measurements. Cores 149-900A-5R through 17R are mainly nannofossil clay and ooze, and have a strong magnetic signal (NRM intensities typically in the range 1 to 10 mA/m) that was easily measured. The magnetic behavior of these sediments is relatively straightforward, with an easily identified characteristic magnetization on the orthogonal demagnetization diagrams (Fig. 12). As shown in Figure 12, although the remanence is still dominated by a single component of magnetization in a majority of the cases, several samples did display a multicomponent nature, with a characteristic component isolated after removal of a secondary component of opposite polarity.

Except for two short intervals, the sediments from 181.5 to 748.9 mbsf were almost always characterized by weak magnetic remanence. We could not measure the discrete samples taken from these sediments accurately, even in a shore-based field-free laboratory. The magnetic directions of these sediments typically become very noisy and inconsistent. Therefore, it was not possible to determine the polarity for the sediments recovered from this interval.

Magnetic Polarity Sequences at Site 900

Table 5 summarizes the paleomagnetic results from Hole 900A. Because biostratigraphic samples between 12.0 and 65.5 mbsf have been assigned ages in the range from 0.8 to 2.6 Ma, the observed predominantly negative inclination in this interval suggest that these sediments were deposited within the Matuyama chron (0.78-2.58 Ma). This match must be the case because the Matuyama is the only reverse chron of this particular age. Between 21.76 and 26.62 mbsf, the cores have been assigned to nannofossil zone NN19f (0.92-1.10 Ma). Therefore, the first shift in polarity from normal to reverse at a depth of 21.08 mbsf would correspond to the onset of the Jaramillo subchron (0.99 Ma) rather than the Brunhes/Matuyama boundary (0.78 Ma). In other words, Hole 900A contains only a partial record of Jaramillo subchron and no record of the Brunhes/Matuyama boundary. The biostratigraphic data also suggest that sediments at about 43.9-48.0 mbsf may be of late Pliocene age (Zones NN19a and N23/N22). This information suggests that the well-defined records of a normal interval (47.00-48.15 mbsf) correspond to the Olduvai normal polarity subchron. As the biostratigraphic data place the cores at a depth of 65.5 mbsf to 2.6 Ma (within Zone NN16), the shift in polarity from reversed to normal at 64.55 mbsf may represent the

Table 3. Paleomagnetic results from Hole 898A used to determine the magnetostratigraphy at Site 898.

Core, section, interval (cm)	Depth (mbsf)	NRM intensity (mA/m)	AF demag step (mT)	Inclination (°)	Polarity
149-898A-					
1H-6, 15–17	7.65	14.2	80	38	N
2H-4, 15–17	13.85	7.1	80	51.4	N
2H-4, 74–76	14.44	7.64	80	66.4	N
3H-3, 52–54	22.24	7.61	80	36.1	N
3H-4, 20–22	23.42	6.65	80	59.3	N
3H-6, 59–61	26.81	13.3	80	22.4	N
4H-1, 86–88	29.06	10.4	30	–53.2	R
4H-2, 108–110	30.78	24.3	80	–69.5	R
4H-4, 93–95	33.63	5.98	80	–55.9	R
4H-5, 121–123	35.41	24.3	80	–75.9	R
4H-6, 8–10	35.78	3.82	80	–73.6	R
4H-6, 89–91	36.59	12.3	80	–61.9	R
5H-1, 76–78	38.46	9.84	30	–30.8	R
5H-1, 143–145	39.13	14.4	70	–52.6	R
5H-2, 10–12	39.3	7.38	70	–45.7	R
5H-3, 129–131	41.99	4.16	99	–19.3	R
5H-3, 134–136	42.04	3.75	80	–40.3	R
5H-4, 59–61	42.82	2.11	60	–41	R
5H-5, 24–26	43.97	3.9	50	–16.5	R
5H-5, 57–59	44.3	3.77	80	–65.2	R
5H-6, 31–33	45.55	5.84	70	–61.9	R
5H-6, 56–58	45.8	4.36	60	–59.1	R
5H-7, 15–17	46.9	2.02	60	–60.3	R
6H-2, 10–12	48.81	5.3	60	–54.6	R
6H-2, 124–126	49.95	2.66	60	–58.2	R
6H-3, 69–71	50.9	0.49	60	–44.7	R
6H-4, 63–65	52.34	0.13	40	–3.4	R?
6H-4, 117–119	52.88	0.37	50	–47	R
6H-5, 27–29	53.49	1.02	50	–33.3	R
6H-6, 136–139	56.08	0.06	30	–36.5	R
6H-7, 17–19	56.39	0.4	40	–46.2	R
6H-7, 29–32	56.51	0.09	40	–30.6	R
7H-3, 62–64	60.32	0.11	80	–31.8	R
7H-7, 1–3	65.71	2.35	30	–10.2	R?
8H-3, 32–34	69.55	2.28	70	–43.3	R
8H-7, 16–18	75.42	22.1	90	–52.9	R
8H-7, 23–25	75.49	10	70	–48.4	R
9H-1, 40–42	76.1	0.19	65	–52.8	R
10H-3, 93–95	89.13	0.09	60	–63.5	R
10H-5, 31–33	91.51	0.23	60	–63.1	R
11H-1, 45–47	95.15	2.5	70	–56.6	R
11H-2, 43–45	96.65	5.58	50	–51.4	R
11H-3, 28–30	98	3.86	30	–20.2	R
11H-4, 43–45	99.65	5.02	80	–59.6	R
11H-5, 102–104	101.74	7.3	30	17.3	N
12H-1, 108–110	105.28	3.05	60	58.6	N
12H-1, 144–146	105.64	9.35	65	–12.9	N?
12H-2, 0–	105.7	17.24	20	48.8	N
12H-2, 2–	105.72	21.33	20	40.1	N
12H-2, 4–	105.74	8.82	35	47.7	N
12H-2, 6–	105.76	1	35	58.5	N
12H-2, 8–	105.78	0.83	20	32.7	N
12H-2, 10–	105.8	1.14	20	36.6	N
12H-2, 12–	105.82	3	20	19.1	N
12H-2, 14–	105.84	1.23	35	33.6	N
12H-2, 16–	105.86	3.97	25	36	N
12H-2, 18–	105.88	4.51	40	–8.3	N?
12H-2, 20–	105.9	1.92	20	37.7	N
12H-2, 22–	105.92	0.98	20	49.8	N
12H-2, 24–	105.94	4.41	20	39.7	N
12H-2, 26–	105.96	3.23	30	49.7	N
12H-2, 28–	105.98	3.26	20	39.8	N
12H-2, 30–	106	3.37	20	24.2	N
12H-2, 32–	106.02	4.71	40	53.7	N
12H-2, 34–	106.04	4.93	20	22.9	N
12H-2, 36–	106.06	5.83	35	36.5	N
12H-2, 38–	106.08	1.01	50	33.1	N
12H-2, 40–	106.1	0.86	30	32.5	N
12H-2, 42–	106.12	1.6	30	37.1	N
12H-2, 44–	106.14	3.11	30	36.3	N
12H-2, 46–	106.16	1.84	35	50.4	N
12H-2, 48–	106.18	1.91	35	40	N
12H-2, 50–	106.2	6.01	50	64.5	N
12H-2, 52–	106.22	6.13	20	38.8	N
12H-2, 54–	106.24	9.32	30	12.3	N
12H-2, 56–	106.26	1.46	20	34.7	N
12H-2, 58–	106.28	0.5	25	19.3	N
12H-2, 60–	106.3	3.68	30	28.7	N
12H-2, 62–	106.32	1.95	30	30.5	N
12H-2, 64–	106.34	1.25	30	35.5	N
12H-2, 66–	106.36	3.3	20	49.52	N
12H-2, 68–	106.38	4.93	20	38.6	N
12H-2, 70–	106.4	1.82	25	8.1	N
12H-2, 72–	106.42	0.82	25	24.4	N
12H-2, 74–	106.44	0.83	25	15	N
12H-2, 76–	106.46	0.78	30	–23.5	R
12H-2, 78–	106.48	2.09	30	–12.1	R
12H-2, 80–	106.5	5.91	25	–20.2	R
12H-2, 82–	106.52	3.35	25	–13.5	R
12H-2, 84–	106.54	2.74	30	6	R?
12H-2, 86–	106.56	1.09	30	4.1	R?
12H-2, 88–	106.58	2.42	30	14.2	R?
12H-2, 90–	106.6	9.13	35	–17.6	R
12H-2, 92–	106.62	7.58	30	5.9	R?
12H-2, 94–	106.64	1.39	30	–2.5	R?
12H-2, 96–	106.66	2.08	30	–4.6	R
12H-2, 98–	106.68	1.51	30	8.6	R?
12H-2, 100–	106.7	5.06	35	–54.1	R
12H-2, 102–	106.72	5.04	20	7.8	N?
12H-2, 104–	106.74	8.03	20	11.3	N?
12H-2, 106–	106.76	5.1	30	–28.1	R
12H-2, 108–	106.78	8.76	30	–43	R
12H-2, 110–	106.8	4.09	30	11.6	N?
12H-2, 112–	106.82	6.78	30	–4.9	R?
12H-2, 114–	106.84	1.07	25	3.6	N?
12H-2, 116–	106.88	1.14	25	–6.2	R?
12H-2, 118–	106.9	12.92	30	–12.1	R?
12H-2, 120–	106.92	13	30	–29.6	R
12H-2, 122–	106.94	5.45	30	–2.5	R?
12H-2, 124–	106.96	2.59	20	–21	R
12H-2, 126–	106.98	14.23	20	–58.2	R
12H-2, 128–	107	2.79	20	–35.4	R
12H-2, 130–	107.02	5.54	20	–11.1	R
12H-2, 132–	107.04	4	30	–49.1	R
12H-2, 134–	107.06	3.96	20	–41.6	R
12H-2, 136–	107.08	9.69	25	–49.8	R
12H-2, 138–	107.1	23.16	30	–50.7	R
12H-2, 140–	107.12	4.53	25	–55.3	R
12H-2, 142–	107.14	3.36	25	–46.4	R
12H-2, 144–	107.16	2.96	25	–70.9	R
12H-2, 146–	107.18	5.39	25	–60.2	R
12H-2, 148–	107.2	5.81	25	–61.9	R
12H-3, 15–17	107.37	6.39	80	–58.8	R
12H-3, 28–30	107.5	5.93	70	43	N
12H-4, 73–75	109.45	0.29	40	–49.6	R
12H-4, 81–83	109.53	0.39	80	–60.2	R
12H-6, 66–68	112.4	2.89	40	–20.9	R
12H-6, 91–93	112.65	0.11	60	–48.4	R
13H-1, 32–34	114.02	15.8	30	–19.4	R
13H-1, 121–123	114.91	0.4	80	–42.5	R
13H-2, 74–76	115.94	12.1	90	–45.2	R
13H-2, 105–107	116.25	1.23	80	–44	R
13H-3, 94–96	117.64	12.1	30	–18.1	R
13H-4, 65–67	118.85	0.08	80	–13	R
13H-5, 23–25	119.93	0.53	60	–58	R
13H-5, 82–84	120.52	0.39	90	–43.2	R
13H-6, 134–136	122.54	0.67	60	–40.7	R
13H-6, 136–138	122.56	0.27	80	–27	R
14H-1, 73–75	123.93	0.43	60	–39	R
14H-2, 139–141	126.1	0.06	40	–31.8	R
14H-3, 12–14	126.35	0.43	60	–52.1	R
14H-4, 84–86	128.6	0.75	40	–49	R
14H-4, 122–124	129.98	0.06	50	–56.6	R
14H-6, 42–44	131.23	0.08	30	–42.3	R
14H-7, 10–12	131.23	0.2	60	–20.4	R
15X-1, 88–90	133.58	0.13	60	–45.7	R
15X-1, 125–127	133.95	0.41	60	–51.2	R
15X-2, 84–86	135.04	0.3	50	–47.8	R
15X-2, 126–128	135.46	0.15	60	–44.3	R
15X-3, 15–17	135.85	0.1	70	–46.1	R
15X-3, 21–23	135.91	0.21	80	–65.6	R
15X-4, 33–35	137.53	0.23	55	2	R?
15X-4, 53–55	137.73	0.04	45	–34.5	R
15X-5, 7–9	138.77	0.12	65	–30.5	R
16X-1, 98–100	139.78	0.21	20	–53.3	R
16X-1, 113–115	139.93	0.21	50	–41.7	R
16X-2, 21–23	140.51	0.35	25	–59.9	R
16X-3, 18–20	141.98	0.07	60	–55.1	R
16X-3, 135–137	143.15	0.28	40	–54.2	R
16X-4, 55–57	143.85	0.09	30	39.8	N
16X-4, 132–134	144.62	0.05	30	–60.9	R
16X-5, 75–77	145.55	6.27	20	–22.6	R
16X-5, 90–92	145.7	0.2	60	–59.5	R
17X-1, 47–49	148.97	0.2	45	14.4	N?
17X-2, 32–34	150.32	0.18	45	–15.7	R
17X-3, 25–27	151.75	0.03	30	–34.9	R
17X-4, 29–31	153.29	0.16	80	–12.9	R?
17X-5, 80–82	155.3	0.3	40	–57.2	R
17X-6, 72–75	156.72	2.52	20	–69.1	R
18X-1, 129–131	159.39	0.28	40	–56.8	R
18X-2, 35–38	159.97	1.67	60	–10.9	R?
18X-2, 95–97	160.57	3.69	40	–44	R
18X-3, 70–72	161.82	4.53	40	17.5	N
18X-4, 25–29	162.87	2.05	60	–5.4	N?
18X-4, 114–116	163.76	0.18	40	6.4	N?
18X-5, 124–126	165.36	14.7	80	–74.2	R
18X-6, 34–36	165.96	16.6	20	–45.2	R
18X-6, 132–134	166.94	12.6	60	29.3	N
18X-7, 8–10	167.2	22.4	60	–53.5	R

Table 3 (continued).

Core, section, interval (cm)	Depth (mbsf)	NRM intensity (mA/m)	AF demag step (mT)	Inclination (°)	Polarity
19X-1, 23–25	168.03	8.57	60	−33.5	R
19X-1, 115–117	168.95	26.7	60	−66.3	R
19X-2, 58–60	169.88	18.5	60	−61.6	R
19X-2, 93–95	170.23	8.61	30	−40.8	R
19X-3, 33–35	171.13	30.2	60	−75.8	R
19X-4, 92–94	173.22	13.4	60	−56.8	R
19X-5, 34–36	174.14	8.62	40	−45.8	R
19X-5, 69–71	174.49	3.52	40	−75.4	R
19X-6, 58–61	175.88	2.53	40	−69.1	R
20X-1, 51–53	177.91	0.05	30	−46.7	R
20X-2, 94–96	179.84	2.35	20	−28.8	R
20X-2, 130–132	180.2	0.06	30	−55.1	R
20X-3, 104–106	181.44	0.08	30	−46.8	R
20X-3, 112–114	181.52	0.04	30	−37.6	R
20X-4, 52–54	182.42	0.03	30	−39.3	R
20X-4, 84–86	182.74	0.03	20	48.4	N
21X-1, 54–56	187.54	5.16	20	−15.8	N?
21X-1, 131–133	188.31	0.06	20	−20.3	R?
21X-2, 65–67	189.15	3.41	50	−35.2	R
21X-2, 93–95	189.43	1.96	20	1.8	R?
21X-3, 75–78	190.75	0.06	20	−31.6	R
21X-3, 133–135	191.33	0.05	30	1.9	R?
21X-4, 53–55	192.03	0.08	25	−11.6	R?
21X-4, 75–77	192.25	0.06	20	−15.6	R?
22X-1, 33–35	197.03	0.07	30	64.9	N
22X-2, 45–47	198.65	1.18	20	25.8	N
22X-3, 90–92	200.6	1.98	20	51.6	N
22X-4, 21–23	201.41	1.59	20	−0.2	N?
22X-4, 131–133	202.51	0.09	40	63.6	N
22X-5, 31–33	203.01	0.05	40	51.4	N
22X-6, 54–56	204.74	0.06	40	36.8	N
22X-6, 98–100	205.18	0.05	40	31	N
22X-7, 12–14	205.82	0.03	60	60.4	N
23X-1, 46–48	206.86	0.09	40	−39	R
23X-2, 40–42	208.3	0.09	20	−63.8	R
23X-2, 79–82	208.69	0.41	30	−60	R
23X-3, 31–33	209.73	0.1	40	−53.2	R
23X-3, 96–99	210.38	0.07	40	−53.6	R

Note: See Table 1 for explanation of abbreviations.

Matuyama/Gauss boundary (2.58 Ma). Like Hole 898A, the Réunion subchron is not observed in Hole 900A. Finally, the lower boundaries of both nannofossil Zone NN15 and foraminiferal Zone N19 have been placed at about 89 mbsf, which would suggest that the sediments at about this depth were deposited within the Gilbert chron (early Pliocene). This biostratigraphically inferred chronostratigraphic event plays crucial role in the interpretation of the magnetic zones identified in the early Pliocene.

Although biostratigraphic age markers are not well defined below a depth of 89.39 mbsf, the magnetic polarity patterns identified from depth interval 76.9-141.85 mbsf allow tentative correlations of the magnetic zones with the GPTS. Within the Gauss chron, the inclinations of the U-channel sample in Core 149-900A-10R at a depth of 77.1 mbsf changed from reversed to normal, which probably recorded the transition of the Mammoth subchron (3.22-3.33 Ma). The Kaena subchron (3.04-3.11 Ma) appears not recorded in Hole 900A. Within the Gilbert reverse chron four thin normal polarity zones between 84.2 and 95.6 mbsf show a good correlation with the Cochiti (4.18-4.29 Ma), Nunivak (4.48-4.62 Ma), Sidufjall (4.80-4.89 Ma), and Thvera (4.98-5.23 Ma) subchrons at depth intervals of 84.2-84.4, 87.1-87.5, 89.3-90.0, and 95.2-95.6 mbsf, respectively. The Gilbert/C3A chron boundary (5.83 Ma) occurs at depth 113.8 mbsf, and the shift in polarity from reversed to normal at a depth of 134.29 mbsf may correspond to Chron C3A/C4 boundary (7.27 Ma). Similarly with the Gilbert chron, the two thin normal zones between 113.8 and 115.8 mbsf, the three normal zones between 121.9 and 132.7 mbsf, and the three normal zones between 134.3 and 145.0 mbsf may be correlated with the corresponding normal polarity intervals in Epochs 5, 6, and 7, respectively. The magnetostratigraphic and biostratigraphic zones at Hole 900A are summarized in Table 6 and the interpretation of the magnetostratigraphy is presented in Figure 13.

Paleomagnetically Determined Sedimentation Rates at Site 900

As indicated in Figure 14, about four separate straight-line segments may be fitted to the paleomagnetic correlation points for Hole 900A (Table 6). This plot of the sediment-accumulation rate shows a change in slope (5.9 m/Ma) near 48 mbsf, above which rates are 37.0 m/Ma and below which rates vary from 23.0 to about 7.2 m/Ma. Between the lower Pliocene at 84.2 mbsf and the uppermost Miocene at 95.2 mbsf is another possible unconformity (Fig. 14). According to this interpretation, two significant sedimentary hiatuses occurred: one is close to the Pliocene-Pleistocene boundary, in an identical position to that proposed at Sites 897 and 898, and the other is in the interval of 4.18-4.89 Ma at about 90 mbsf. It is important to note the absence of direct paleontological evidence for these hiatuses, especially for the proposed Pliocene-Pleistocene hiatus because all standard late Pliocene and Pleistocene calcareous nannoplankton and planktonic foraminiferal zones appear to be present at these sites (Liu and Mariono, this volume; Gervais, this volume). The average sedimentation rates at Site 900 are significantly lower than those of Sites 897 and 898 for the same age range. This may be due to the fact that Site 900 is located near the foot of the Portuguese continental rise adjacent to the Iberia Abyssal Plain. Sediments carried by the turbidity currents may merely pass by, flow down slope, and come to rest at the abyssal plain (e.g., at Sites 898 and 897). This interpretation is in agreement with shipboard geological observation, which suggests that, compared with Sites 897 and 898, much more hemipelagic sediments but less turbidites were found in the recovered cores from Hole 900A (Shipboard Scientific Party, 1994c). On the other hand, the comparatively abrupt changes at a depth of 48 mbsf may suggest the additional influence of other factors. For example, they may be associated with the onset of the Arctic glaciation or increased detrital input resulting from the worldwide regression to the commencement of this glaciation.

DISCUSSION

The characteristic magnetization observed at Holes 897C, 898A, and 900A is of both normal and reversed polarities. Fairly complete magnetostratigraphies were obtained from Sites 897, 898, and 900 for the Pliocene to Pleistocene. Secular variation of the geomagnetic field could not be detected from these sediments because of the drilling-induced remagnetization.

As we emphasized in the "Introduction" section, one has to demonstrate the remanent magnetization of the sediment is the stable primary magnetization acquired at, or close to, deposition before the application of magnetostratigraphy. The precise time at which sediments acquire their magnetization is always difficult to evaluate, and at the present time there is still no universally applicable test that allows a distinction to be made between depositional remanent magnetization (DRM) acquired at the time of deposition and chemical remanent magnetization (CRM) acquired as a result of the growth of new magnetic minerals during diagenesis. However, there is some indirect evidence from the spectrum of unblocking temperatures and coercivity that for most of the samples discussed in this paper, the stable component of magnetization is carried by magnetite, rather than hematite. It is widely believed that titanomagnetites in marine sediments are normally of detrital, rather than chemical, origin because chemically formed iron oxides normally result from the initial precipitation of iron hydroxides, which are later dehydrated to produce hematite rather than magnetite. Thus, as a general rule, CRM in marine sediments tends to reside in hematite grains, which, so far have not been identified in these Cenozoic sediments. Of course, there are mechanisms by which magnetite can be precipitated in marine sediments, so that the possibility of magnetite grains carrying a CRM cannot be completely ruled out. However, we regard this as unlikely

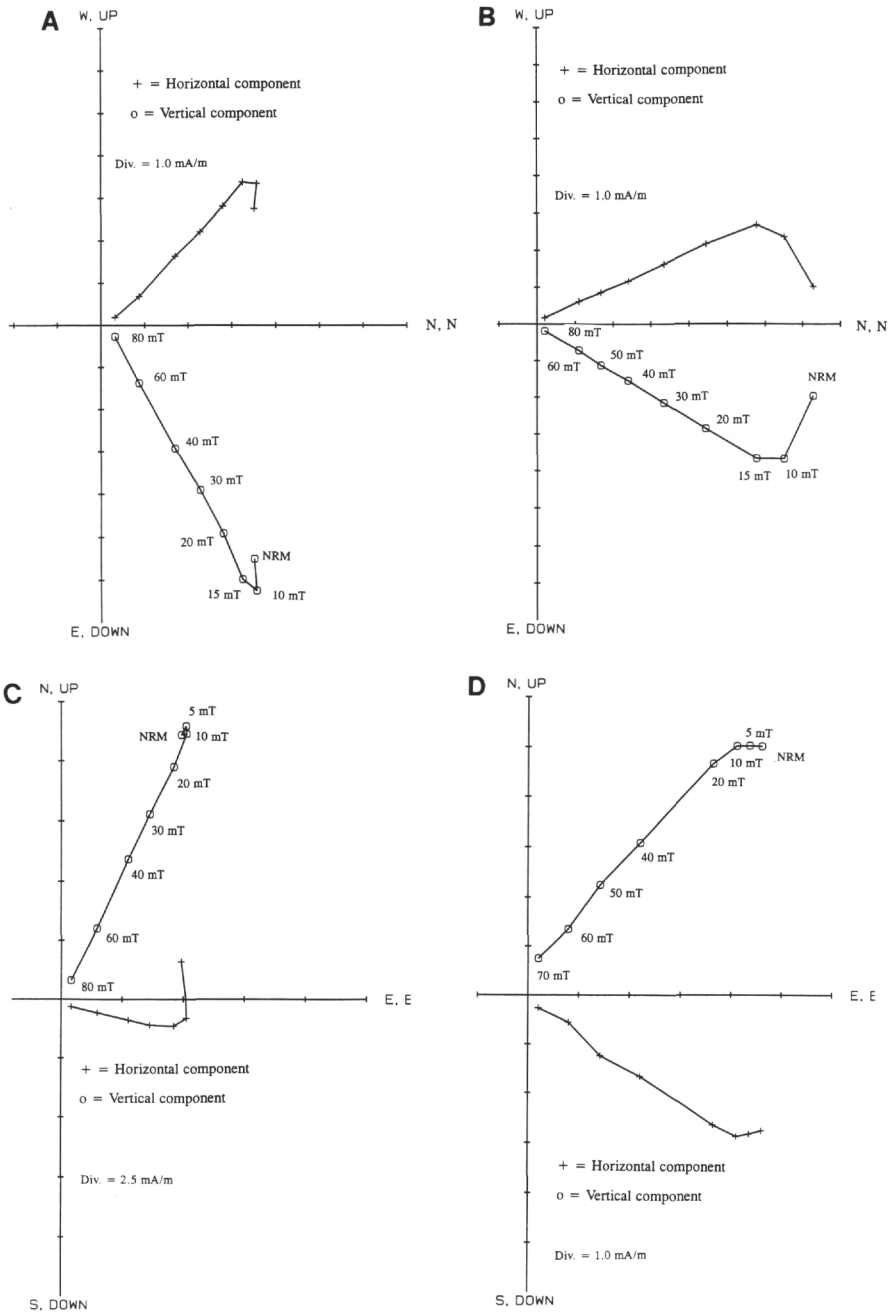

Figure 9. Representative vector end-point diagrams showing the results of AF demagnetization for samples from Site 898. Crosses and circles represent the projection of the magnetization vector end point on the horizontal and vertical planes, respectively. Samples 149-898A-2H-4, 15-17 cm (**A**), and 149-898A-3H-52-54 cm (**B**), show normal polarity of ChRM, whereas Samples 149-898A-4H-6, 89-91 cm (**C**), and 149-898A-5H-2, 10-12 cm (**D**), show reversed polarity ChRM.

in these particular sediments. As shown in Table 7, application of the reversal test on the mean normal and reversed inclinations of the three sites for the upper Pliocene-Pleistocene interval yields positive results on Sites 898 and 900: the two polarity inclinations are not statistically different from each other at the 95% confidence level (C class reversal test results in McFadden and McElhinny (1990)). The positive results from mean inclination reversal test indicates that the ChRM is a record of the paleomagnetic field close to the time of formation of these sediments.

Further evidence that the magnetization of these sediments was acquired close to their time of deposition is the fact that patterns of magnetic reversals have been identified, which can be matched with the established polarity time scale. If the magnetization had been introduced as a result of the variable processes of diagenesis at significantly different times from the initial deposition, such a close match would be unlikely. Finally, most of the observed magnetostratigraphy from the characteristic directions is in excellent agreement with that to be expected from the stratigraphic position of the sequence deduced from the biostratigraphic data. On these bases, it is argued that the characteristic directions of magnetization observed from these sediments are most likely the original primary magnetization acquired when the sediments were deposited.

As with most applications of magnetostratigraphy, one of the greatest problems is the correct matching of the observed sequence of magnetic polarity zones with the appropriate part of the GPST. At Sites 897 and 898, this matching is usually straightforward and un-

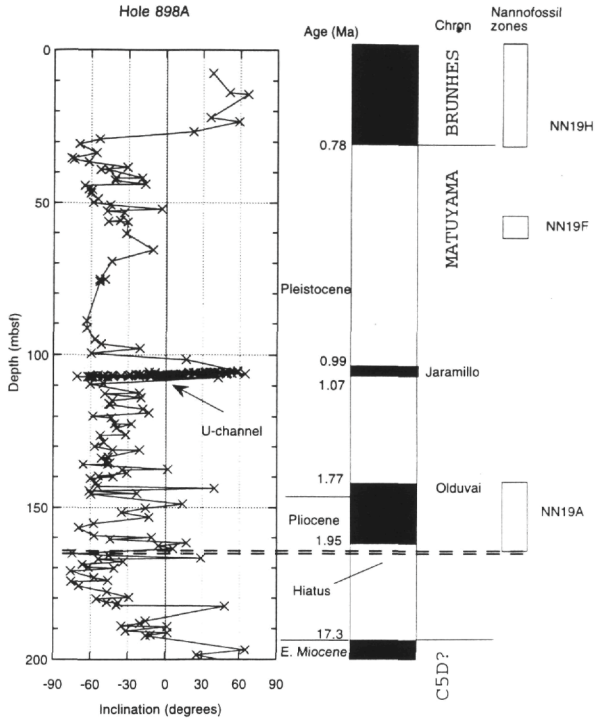

Figure 10. Downhole variation of stable magnetic inclination, inferred polarity and biostratigraphic zones for Cenozoic sediments at Site 898. Normal polarity is indicated by black areas; reversed polarity is indicated by white areas.

ambiguous as the observed polarity sequence is defined from the sedimentary succession that is more or less continuous through to recent time. Thus, in the two sites illustrated in Figures 8 and 11, the youngest normal polarity zone can correlated confidentially with the Brunhes normal chron, the preceding dominantly reverse polarity zone with the Matuyama reverse chron, and so on through the sequence. For Site 900, the available sedimentary section is not continuous through to the present, hence, the interpretation of the paleomagnetic record is less straightforward. However, available biostratigraphic data from this site can assist in deciding which observed magnetic polarity zone or set of zones should be correlated with which magnetic chron on the GPST, such as the match with the Matuyama reverse chron discussed above. This combined paleomagnetic, biostratigraphic, and sedimentological study has demonstrated the potential value of providing the essential link between the biostratigraphic and geomagnetic polarity time scales.

The patterns of magnetic polarity reversals identified at Sites 897, 898, and 900 correlate well with the known magnetic polarity time scale for the past 5 Ma, and allow the determination of accurate sediment-accumulation rates for these sites (Fig. 8, 11, and 14). These sedimentation rate values are not corrected for compaction, and consequently part of the apparent series of increases in accumulation rates for the interval of 2-2.5 Ma at Sites 897 and 898 may be attributed to this cause. The identification of the early Pleistocene hiatus at all three sites suggests the occurrence of a contemporaneous oceanographic event, the influence of which may have been sufficiently widespread to affect much of the Iberia Abyssal Plain and is probably associated with the Pleistocene glaciation.

As can be seen from Tables 1, 3, and 5, we present here the magnetic polarity stratigraphy determined for only a small portion of the total recovered section in Cenozoic. The paleomagnetic results from other portions cannot be interpreted with confidence because of the weak magnetization. As mentioned previously, there is a magnetic boundary where NRM intensity sharply decreases in all three sites. At Hole 897C this magnetic boundary occurs at a depth of 334 mbsf, at Hole 898A it occurs at a depth of 197 mbsf, and at Hole 900A it is at a depth of 146 mbsf. In all three cases this change is reasonably well defined stratigraphically, within the middle Miocene nannofossil Zones NN5-NN8 (de Kaenel and Bergen, this volume), indicating that it may represent a synchronous event at the three sites. It is also significant to note that at all three holes this abrupt decrease in NRM intensity also correlates precisely with a sharp reduction in magnetic susceptibility (see Shipboard Scientific Party, 1994). Both of the NRM intensity and magnetic susceptibility are parameters that likely reflect variations in type and amount of magnetic minerals within the sediments, but because the NRM intensity may also be a function of other factors, such as geomagnetic field intensity at the time of deposition and secondary magnetization acquired during drilling or storage, susceptibility is a more useful index of magnetic mineral content. In this study, there is a high probability that both parameters reflect variations in the proportion of terrigenous magnetite owing to changes in either source area, sediment supply rate, or rate of dissolution of the nonmagnetic component (calcareous and siliceous). Because the dominant magnetic mineral in these sediments is magnetite, most probably of detrital origin, this sharp decrease in susceptibility and NRM intensity appears to represent an abrupt reduction in the rate of supply of terrigenous material at the middle Miocene. Preliminary shipboard data also indicate that at these depths where the both NRM intensity and susceptibility decrease, there is also a transition from oxidized iron phased in the Miocene brown clays to reduced iron phases in the late Oligocene age green and gray clays (Shipboard Scientific Party, 1994a-c). The suggested boundary between oxidized and reduced iron phases corresponds to the top of a region of high sulfate concentration, which is apparent in the interstitial-water analyses (see "Inorganic Geochemistry" sections, Shipboard Scientific Party, 1994a-c). The terminated supply of terrigenous material at the end of the early Miocene may reflect the occurrence of an important oceanographic or tectonic event at this time, which resulted in a change in circulation patterns, sediment supply routes, or sources areas within the Iberia Abyssal Plain. This interpretation is fully consistent with the middle Miocene regional unconformity found in much of western Iberia. This unconformity is believed to be the result of a northwest-southeast compressional folding in the Beti mountains of southern Spain (Mauffret et al., 1989).

It is of interest to note that this magnetic boundary (weak NRM intensity and susceptibility) not only provides a proxy stratigraphic marker for correlation between the sedimentary records of drilled sites during Leg 149, but also reveals the middle Miocene folding event that is synchronous at the three sites.

CONCLUSIONS

This combined study has demonstrated the potential value of shipboard paleomagnetic, biostratigraphic and sedimentological investigations in providing the essential link between the biostratigraphic and geomagnetic polarity time scales. Sedimentary sections of late Neogene age from Sites 897, 898, and 900 have recorded a pattern of magnetic polarity reversals that correlates well with the known magnetic polarity time scale for the past 5 Ma, and allows the determination of accurate sediment-accumulation rates. A short but maybe significant hiatus in the lower Pleistocene was recognized at all three sites. This hiatus may represent an oceanographic event that affected a significant part of the Iberia Abyssal Plain region. Because of the limited resolution of available micropaleontological zonations, this hiatus could not have been detected by biostratigraphic observations alone. Downhole magnetic susceptibility and intensity values provide a useful basis for correlation of the sudden decrease in magnetic signal, which may be caused by the termination in supply of the terrigenous material in middle Miocene and reflects the occurrence of the tectonic folding event at this time in much of western Iberia. It is

clear from this study that the combination of paleomagnetic and biostratigraphic studies on the same deep-sea sediment cores can provide important information that has considerable relevance to understanding the evolution of continental margins.

ACKNOWLEDGMENTS

We thank Bob Whitmarsh, Dale Sawyer, and other shipboard scientists, the ODP marine technicians, and both captain and crews of the *JOIDES Resolution* for their help and company during Leg 149, and Wuchang Wei for providing a preprint of his results. We gratefully acknowledge Neil Opdyke and Wulf Gose for insightful reviews of this manuscript. Special thanks go to Neil Opdyke who provided valuable advice and improved this paper. This research was supported by a grant to X.Z. from the U.S. Science Support Program of the Joint Oceanographic Institutions, Inc., and by grants to D.M. from the Natural Environment Research Council, United Kingdom (GST/02/725) and the EC MAST program (MAS2-CT94-0083). This paper is also Institute of Tectonic of UCSC contribution no. 268.

REFERENCES

Cande, S.C., and Kent, D.V., 1992. A new geomagnetic polarity time scale for the Late Cretaceous and Cenozoic. *J. Geophys. Res.,* 97:13917-13951.

———, 1995. Revised calibration of the geomagnetic polarity time scale for the Late Cretaceous and Cenozoic. *J. Geophys. Res.,* 100:6093-6095.

Clement, B.M., and Kent, D.V., 1987. Short polarity intervals within the Matuyama: transitional field records from hydraulic piston core sites from the North Atlantic. *Earth Planet. Sci. Lett.,* 81:253-264.

Fisher, R.A., 1953. Dispersion on a sphere. *Proc. R. Soc. London A,* 217:295-305.

Hilgen, F.J., 1991. Astronomical calibration of Gauss to Matuyama sapropels in the Mediterranean and implication for the geomagnetic polarity time scale. *Earth Planet. Sci. Lett.,* 104:226-244.

Kirschvink, J.L., 1980. The least-squares line and plane and analysis of palaeomagnetic data. *Geophys. J. R. Astron. Soc.,* 62:699-718.

Mankinen, E.A., Donnelly, J.M., and Grommé, C.S., 1978. Geomagnetic polarity event recorded at 1.1 m.y. B.P. on Cobb Mountain, Clear Lake volcanic field, California. *Geology,* 6:653-656.

Mankinen, E.A., and Grommé, C.S., 1982. Paleomagnetic data from the Coso Range, California, and the current status of the Cobb Mountain normal geomagnetic event. *Geophys. Res. Lett.,* 9:1279-1282.

Mauffret, A., Mougenot, D., Miles, P.R., and Malod, J.A., 1989. Cenozoic deformation and Mesozoic abandoned spreading centre in the Tagus abyssal plain (west of Portugal): results of a multichannel seismic survey. *Can. J. Earth Sci.,* 26:1101-1123.

McFadden, P.L., and McElhinny, M.W., 1990. Classification of the reversal test in palaeomagnetism. *Geophys. J. Int.,* 103:725—729.

McFadden, P.L., and Reid, A.B., 1982. Analysis of paleomagnetic inclination data. *Geophys. J. R. Astron. Soc.,* 69:307-319.

McKenzie, D., 1978. Some remarks on the development of sedimentary basins. *Earth Planet. Sci. Lett.,* 40:25-32.

Sawyer, D.S., Whitmarsh, R.B., Klaus, A., et al., 1994. *Proc. ODP, Init. Repts.,* 149: College Station, TX (Ocean Drilling Program).

Shackleton, N.J., Berger, A., and Peltier, W.A., 1990. An alternative astronomical calibration of the lower Pleistocene timescale based on ODP Site 677. *Tram. R. Soc. Edinburgh: Earth Sci.,* 81:251-261.

Shipboard Scientific Party, 1994a. Site 897. *In* Sawyer, D.S., Whitmarsh, R.B., Klaus, A., et al., *Proc. ODP, Init. Repts.,* 149: College Station, TX (Ocean Drilling Program), 41-113.

———, 1994b. Site 898. *In* Sawyer, D.S., Whitmarsh, R.B., Klaus, A., et al., *Proc. ODP, Init. Repts.,* 149: College Station, TX (Ocean Drilling Program), 115-146.

———, 1994c. Site 900. *In* Sawyer, D.S., Whitmarsh, R.B., Klaus, A., et al., *Proc. ODP, Init. Repts.,* 149: College Station, TX (Ocean Drilling Program), 211-262.

Spell, T.L., and McDougall, I., 1992. Revisions to the age of the Brunhes-Matuyama boundary and the Pleistocene geomagnetic polarity timescale. *Geophys. Res. Lett.,* 19:1181-1184.

Wei, W.C., 1995. Revised age calibration points for the geomagnetic polarity time scale. *Geophys. Res. Lett.,* 22:957-960.

Zhao, X., Roperch, P., and Stokking, L.B., 1994. Magnetostratigraphy of the North Aoba Basin. *In* Greene, H.G., Collot, J.-Y., Stokking, L.B., et al., *Proc. ODP, Sci. Results,* 134: College Station, TX (Ocean Drilling Program), 457-474.

Zijderveld, J.D.A., 1967. AC demagnetization of rocks: analysis of results. *In* Collinson, D.W., Creer, K.M., and Runcorn, S.K. (Eds.), *Methods in Palaeomagnetism:* New York (Elsevier), 254-286.

Date of initial receipt: 5 December 1994
Date of acceptance: 26 June 1995
Ms 149SR-212

Table 4. Paleomagnetic and biostratigraphic datums at Hole 898A.

Magnetic datum (chron or subchron)	Biostratigraphic datums (N, F)	Age (Ma)		Depth range (mbsf)	
		(magnetism)	(biostratrigraphy)	(magnetism)	(biostratigraphy)
Brunhes/Matuyama	NN19h, N23/N22	0.78	0.48–0.83	29.06	20.34–47.20
Jaramillo	NN19f	0.99–1.07	0.89–1.06	101.74–106.88	54.69–59.77
Olduvai	NN19a	1.77–1.95	1.66–1.91	143.85–161.82	144.33–163.18
C5D?	N7/N6	17.31–17.65	E. Miocene	197.03–205.82	196.7–206.4

Notes: N = nannofossil, F = foraminiferal datums.

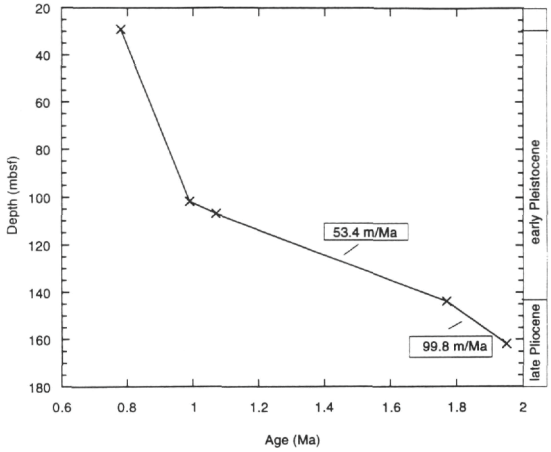

Figure 11. Depth vs. age curve for Hole 898A. The paleomagnetic data points are listed in Table 4. Note the short hiatus, or a decrease in accumulation rate, again inferred within the interval 1.4 to 1.95 Ma.

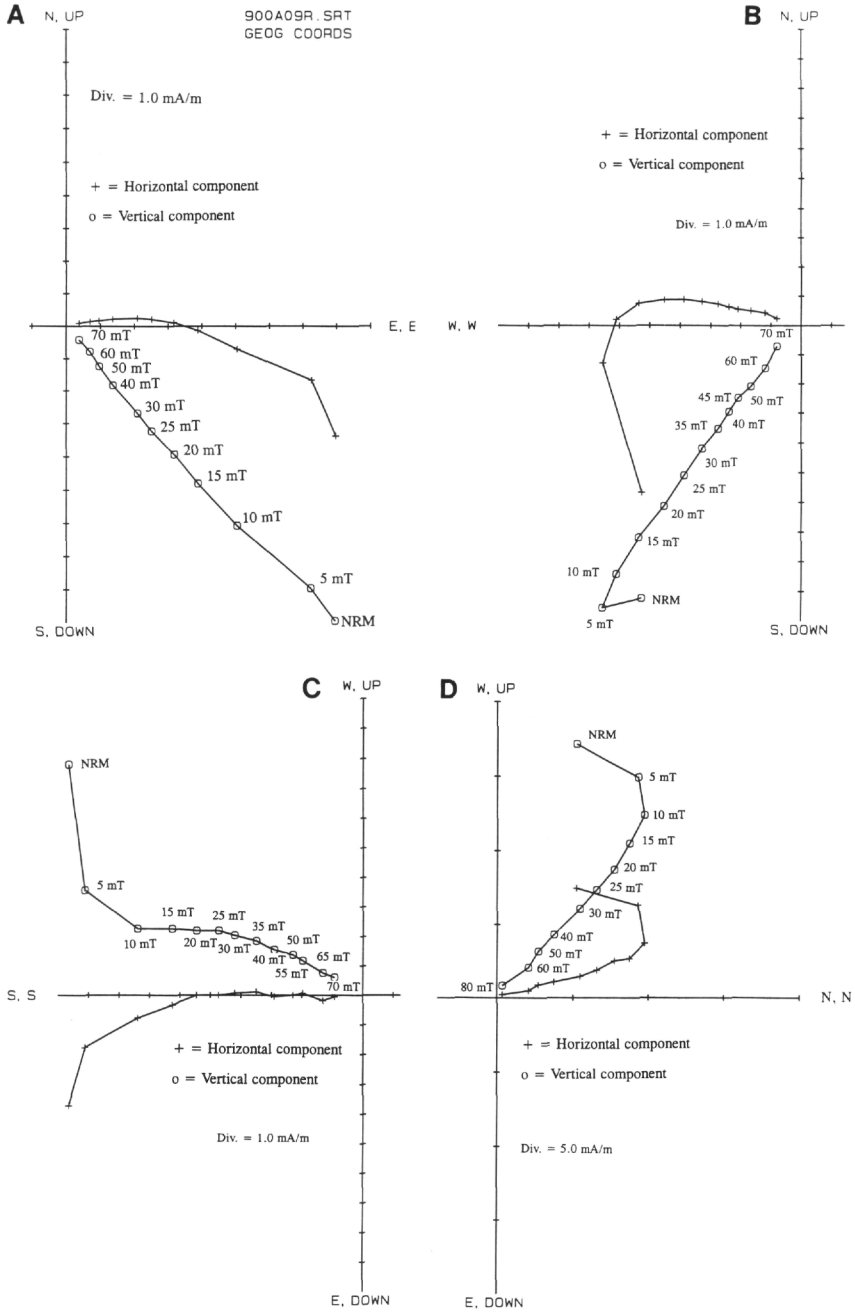

Figure 12. Representative vector end-point diagrams showing the results of AF demagnetization for samples from Site 900. Crosses and circles represent the projection of the magnetization vector end point on the horizontal and vertical planes, respectively. Samples 149-900A-9R-3, 35-37 cm (**A**), and 149-900A-10R-2, 70-72 cm (**B**), show normal polarity of ChRM, whereas Samples 149-900A-10R-5, 7-9 cm (**C**), and 149-900A-14R-5, 107-109 cm (**D**), show reversed polarity of ChRM.

Table 5. Paleomagnetic results from Hole 900A used to determine magnetostratigraphy at Site 900.

Core, section, interval (cm)	Depth (mbsf)	NRM intensity (mA/m)	AF demag step (mT)	Inclination (°)	Polarity
149-900A-					
4R-1, 7–9	20.87	2.7	80	20.6	N
4R-1, 28–30	21.08	14	90	40.5	N
5R-1, 27–29	30.67	5	70	−35.2	R
5R-1, 34–36	30.74	16	70	−62.1	R
5R-1, 96–98	31.36	4	60	−6	R
5R-2, 27–29	32.17	10	60	−53.3	R
5R-2, 30–32	32.2	16	70	−52.3	R
6R-4, 38–40	44.88	3.8	99	−48.4	R
6R-4, 95–97	45.45	10	60	−69.1	R
6R-5, 45–47	46.45	46	80	−63.7	R
6R-5, 95–97	46.95	3.1	65	−48.3	R
6R-5, 100–102	47	6.7	50	32.7	N
6R-6, 50–52	48	5.8	25	36	N
6R-6, 56–58	48.06	18.7	80	34.3	N
6R-6, 104–106	48.54	3.7	99	−53.1	R
7R-1, 51–53	50.11	7.2	70	−37.3	R
7R-1, 116–118	50.76	7.9	70	−42.3	R
7R-2, 28–30	51.38	10.9	70	−43	R
7R-2, 31–33	51.41	9.3	70	−51.7	R
7R-3, 4–7	52.64	12.7	80	−31.9	R
7R-6, 33–35	57.43	9	80	−39.7	R
8R-1, 9–11	59.39	18.1	70	−43.7	R
8R-1, 17–19	59.47	19	70	−56.1	R
8R-3, 72–74	63.02	5.9	60	−30.5	R
8R-3, 80–82	63.1	18	70	−26.5	R
8R-3, 83–85	63.13	13.5	70	−55.2	R
9R-1, 5–7	64.55	11.2	45	29	N
9R-1, 67–69	65.17	10.4	70	28.8	N
9R-1, 76–78	65.26	10.6	70	18.2	N
9R-2, 40–42	66.4	4.46	80	34.4	N
9R-2, 114–116	67.14	9.49	50	65.4	N
9R-3, 10–12	67.6	22	70	30.6	N
9R-3, 33–35	67.83	12	70	52.1	N
10R-1, 61–63	74.71	8.27	60	52.3	N
10R-1, 94–96	75.04	14.2	70	39	N
10R-2, 35–37	75.95	10.6	80	54.1	N
10R-2, 70–72	76.3	12	70	51.2	N
10R-2, 130–132	76.9	3.24	70	−53.8	R
10R-3, 1–	77.1	7.82	35	−45.6	R
10R-3, 3–	77.12	6.75	20	−49.5	R
10R-3, 5–	77.14	11	20	−50	R
10R-3, 7–	77.16	2.95	25	−21.8	R
10R-3, 11–	77.18	5.29	25	−14.2	R
10R-3, 13–	77.2	5.41	30	−24.1	R
10R-3, 15–	77.22	3.18	20	−15.3	R
10R-3, 18–	77.24	5.12	30	−5.8	R
10R-3, 20–	77.26	4.65	20	−14.6	R
10R-3, 22–	77.28	5.71	20	−16.9	R
10R-3, 25–	77.3	7.73	35	−16	R
10R-3, 28–	77.32	10.47	30	52	N
10R–3, 31–	77.34	8.78	35	−17.8	R
10R-3, 34–	77.36	7.71	20	−11	R
10R-3, 36–	77.38	5.64	25	−14.8	R
10R-3, 38–	77.4	5.6	35	−15.8	R
10R-3, 41–	77.42	10.15	20	−7.4	R
10R-3, 43–	77.44	8.63	20	−23.5	R
10R-3, 45–	77.46	2.17	25	−38.6	R
10R-3, 49–	77.48	5.46	25	−15.3	R
10R-3, 51–	77.5	7.1	20	−15.3	R
10R-3, 53–	77.52	7.9	20	−15.7	R
10R-3, 57–	77.54	6.15	20	−8.4	R
10R-3, 60–	77.56	8.26	20	−7.2	R
10R-3, 62–	77.58	4.94	25	−31.3	R
10R-3, 64–	77.6	4.56	35	−36.3	R
10R-3, 66–	77.62	8.75	20	−24.9	R
10R-3, 68–	77.64	4.71	20	−57.5	R
10R-3, 70–	77.66	6.76	20	−14.1	R
10R-3, 72–	77.68	17.52	35	−43.2	R
10R-3, 75–	77.7	6.37	20	−19.9	R
10R-3, 78–	77.72	4.58	20	55.3	N
10R-3, 82–	77.74	4.94	20	11.2	N
10R-3, 84–	77.76	6.09	30	59.4	N
10R-3, 86–	77.78	6.11	20	−13.8	R
10R-3, 89–	77.8	5.35	30	−19.5	R
10R-3, 92–	77.82	4.28	25	−78.4	R
10R-3, 94–	77.84	6.62	25	−39.4	R
10R-3, 96–	77.86	5.67	25	−35.9	R
10R-3, 98–	77.88	5.72	25	−43.1	R
10R-3, 100–	77.9	5.97	25	−39	R
10R-3, 102–	77.92	3.55	25	−42.2	R
10R-3, 104–	77.94	7.28	20	−26.9	R
10R-3, 106–	77.96	5.02	20	−12.5	R
10R-3, 108–	77.98	7.53	20	−8.3	R
10R-3, 110–	78	7.67	20	0.9	R?
10R-3, 112–	78.02	6.7	20	−15.4	R
10R-3, 114–	78.04	2.99	30	−35.4	R
10R-3, 116–	78.06	3.52	25	−41.2	R
10R-3, 118–	78.1	3.24	25	−79.1	R
10R-3, 120–	78.12	2.46	25	−69.4	R
10R-3, 122–	78.14	4.13	25	−30.8	R
10R-3, 124–	78.16	4.86	25	−27.6	R
10R-3, 126–	78.18	4.39	20	20.3	N
10R-3, 128–	78.2	3.26	20	20.9	N
10R-3, 130–	78.22	6.42	35	33.4	N
10R-3, 132–	78.24	5.24	20	−38.7	R
10R-3, 134–	78.26	6.84	20	−57.6	R
10R-3, 136–	78.28	6.93	20	−48.7	R
10R-3, 138–	78.3	3.13	20	−33.9	R
10R-3, 140–	78.32	1.22	25	−24.2	R
10R-3, 142–	78.34	2.4	34	−2.4	R
10R-3, 144–	78.36	3.54	34	4.4	N
10R-3, 146–	78.38	2.61	25	19.5	N
10R-3, 148–	78.38	4.7	25	24	N
10R-4, 7–9	78.67	3.82	70	66.9	N
10R-4, 59–61	79.19	4.82	70	−49.6	R
10R-4, 139–141	79.99	3	70	−76.1	R
10R-5, 4–6	80.14	13	70	−28.1	R
11R-1, 14–16	83.84	16.2	80	−48.1	R
11R-1, 52–54	84.22	4.48	80	18.6	N
11R-1, 65–67	84.35	7.99	80	−31.5	R
11R-2, 79–81	85.99	11.1	80	−68.1	R
11R-2, 98–100	86.18	10.4	80	−60.3	R
11R-3, 40–42	87.1	11	80	60.6	N
11R-3, 75–77	87.45	6.93	95	32	N
11R-4, 10–12	88.3	5.9	80	−51.6	R
11R-4, 110–112	89.3	13.2	80	38.6	N
11R-5, 2–4	89.72	7	80	35	N
11R-5, 29–31	89.99	30.8	80	66.7	N
12R-1, 71–73	94.11	12.8	99	−49.6	R
12R-1, 127–129	94.67	9.94	50	−56.8	R
12R-2, 32–34	95.22	8.86	75	51.4	N
12R-2, 70–72	95.6	7.04	80	38.7	N
12R-3, 69–71	97.09	11.1	70	−65.9	R
12R-3, 84–86	97.24	12.6	70	−43.4	R
14R-1, 15–17	112.85	19	80	−35.7	R
14R-1, 110–112	113.8	28.4	80	15	N
14R-1, 133–135	114.03	18.7	80	46.8	N
14R-2, 39–41	114.59	4.41	70	15.6	N
14R–2, 87-89	115.07	5.49	80	−56.1	R
14R-2, 126–128	115.46	13.6	80	42.6	N
14R-3, 13–15	115.83	14.4	80	66.9	N
14R-3, 89–91	116.59	16.3	99	-43.2	R
14R-3, 126–128	116.96	6.91	80	−51.8	R
14R-4, 24–26	117.44	5.09	80	−65	R
14R-4, 67–69	117.87	10.3	70	−61.1	R
14R-4, 91–93	118.11	8.31	80	−48.7	R
14R-5, 32–34	119.02	19.6	90	−55.1	R
14R-5, 107–109	119.77	19.4	80	−48.6	R
14R-5, 119–121	119.89	13.1	80	−59.2	R
14R-6, 14–16	120.34	8.87	70	−20.2	R
14R-6, 92–94	121.12	5.77	70	−24.7	R
14R-6, 140–142	121.6	1.7	80	−12.7	R
14R-7, 19–21	121.89	1.12	80	55.9	N
15R-1, 113–115	123.53	15.2	80	27.2	N
15R-1, 128–130	123.68	6.72	80	53.1	N
15R-2, 26–28	124.16	8.98	80	25.8	N
15R-2, 87–89	124.77	4.62	70	-66	R
15R–2, 128–130	125.18	8.31	99	−42.7	R
15R-3, 56–58	125.96	7.06	90	−53.5	R
15R-3, 65–67	126.05	8.08	90	−61.3	R
15R-3, 137–139	126.77	3.12	80	74.5	N
15R-4, 25–27	127.15	8.8	60	−62.6	R
16R-1, 33–35	132.33	0.05	20	42.4	N
16R-1, 72–74	132.72	5.97	70	−14.2	R
16R-2, 79–81	134.29	0.05	30	55.7	N
16R-2, 115–117	134.65	4.26	80	50.5	N
16R-3, 38–40	135.38	0.06	40	43.3	N
16R-3, 120–122	136.2	0.19	60	−15.7	R
16R-4, 14–16	136.64	0.87	95	−18.9	R
16R-4, 76–78	137.26	3.83	60	−45.7	R
16R-5, 27–29	138.27	11.7	60	38.6	N
16R-5, 39–41	138.39	2.02	80	46.3	N
16R-6, 42–44	139.92	7.53	80	34.2	N
16R-6, 101–103	140.51	0.19	55	41.7	N
17R-1, 25–27	141.85	2.41	80	−42.3	R
17R-1, 107–109	142.67	2.39	40	−53.4	R
17R-2, 24–26	143.34	0.06	15	−21.9	R
17R-2, 37–39	143.47	4.52	70	−40	R
17R-3, 20–22	144.8	4.43	90	−64.2	R
17R-3, 36–38	144.96	0.09	15	80	N?
149-900A-					
4R-1, 7–9	20.87	2.7	80	20.6	N
4R-1, 28–30	21.08	14	90	40.5	N
5R-1, 27–29	30.67	5	70	−35.2	R
5R-1, 34–36	30.74	16	70	−62.1	R
5R-1, 96–98	31.36	4	60	−6	R
5R-2, 27–29	32.17	10	60	−53.3	R
5R-2, 30–32	32.2	16	70	−52.3	R
6R-4, 38–40	44.88	3.8	99	−48.4	R

Table 5 (continued).

Core, section, interval (cm)	Depth (mbsf)	NRM intensity (mA/m)	AF demag step (mT)	Inclination (°)	Polarity
6R-4, 95–97	45.45	10	60	–69.1	R
6R-5, 45–47	46.45	46	80	–63.7	R
6R-5, 95–97	46.95	3.1	65	–48.3	R
6R-5, 100–102	47	6.7	50	32.7	N
6R-6, 50–52	48	5.8	25	36	N
6R-6, 56–58	48.06	18.7	80	34.3	N
6R-6, 104–106	48.54	3.7	99	–53.1	R
7R-1, 51–53	50.11	7.2	70	–37.3	R
7R-1, 116–118	50.76	7.9	70	–42.3	R
7R-2, 28–30	51.38	10.9	70	–43	R
7R-2, 31–33	51.41	9.3	70	–51.7	R
7R-3, 4–7	52.64	12.7	80	–31.9	R
7R-6, 33–35	57.43	9	80	–39.7	R
8R-1, 9–11	59.39	18.1	70	–43.7	R
8R-1, 17–19	59.47	19	70	–56.1	R
8R-3, 72–74	63.02	5.9	60	–30.5	R
8R-3, 80–82	63.1	18	70	–26.5	R
8R-3, 83–85	63.13	13.5	70	–55.2	R
9R-1, 5–7	64.55	11.2	45	29	N
9R-1, 67–69	65.17	10.4	70	28.8	N
9R-1, 76–78	65.26	10.6	70	18.2	N
9R-2, 40–42	66.4	4.46	80	34.4	N
9R-2, 114–116	67.14	9.49	50	65.4	N
9R-3, 10–12	67.6	22	70	30.6	N
9R-3, 33–35	67.83	12	70	52.1	N
10R-1, 61–63	74.71	8.27	60	52.3	N
10R-1, 94–96	75.04	14.2	70	39	N
10R-2, 35–37	75.95	10.6	80	54.1	N
10R-2, 70–72	76.3	12	70	51.2	N
10R-2, 130–132	76.9	3.24	70	–53.8	R
10R-3, 1–	77.1	7.82	35	–45.6	R
10R-3, 3–	77.12	6.75	20	–49.5	R
10R-3, 5–	77.14	11	20	–50	R
10R-3, 7–	77.16	2.95	25	–21.8	R
10R-3, 11–	77.18	5.29	25	–14.2	R
10R-3, 13–	77.2	5.41	30	–24.1	R
10R-3, 15–	77.22	3.18	20	–15.3	R
10R-3, 18–	77.24	5.12	30	–5.8	R
10R-3, 20–	77.26	4.65	20	–14.6	R
10R-3, 22–	77.28	5.71	20	–16.9	R
10R-3, 25–	77.3	7.73	35	–16	R
10R-3, 28–	77.32	10.47	30	52	N
10R-3, 31–	77.34	8.78	35	–17.8	R
10R-3, 34–	77.36	7.71	20	–11	R
10R-3, 36–	77.38	5.64	25	–14.8	R
10R-3, 38–	77.4	5.6	35	–15.8	R
10R-3, 41–	77.42	10.15	20	–7.4	R
10R-3, 43–	77.44	8.63	20	–23.5	R
10R-3, 45–	77.46	2.17	25	–38.6	R
10R-3, 49–	77.48	5.46	25	–15.3	R
10R-3, 51–	77.5	7.1	20	–15.3	R
10R-3, 53–	77.52	7.9	20	–15.7	R
10R-3, 57–	77.54	6.15	20	–8.4	R
10R-3, 60–	77.56	8.26	20	–7.2	R
10R-3, 62–	77.58	4.94	25	–31.3	R
10R-3, 64–	77.6	4.56	35	–36.3	R
10R-3, 66–	77.62	8.75	20	–24.9	R
10R-3, 68–	77.64	4.71	20	–57.5	R
10R-3, 70–	77.66	6.76	20	–14.1	R
10R-3, 72–	77.68	17.52	35	–43.2	R
10R-3, 75–	77.7	6.37	20	–19.9	R
10R-3, 78–	77.72	4.58	20	55.3	N
10R-3, 82–	77.74	4.94	20	11.2	N
10R-3, 84–	77.76	6.09	30	59.4	N
10R-3, 86–	77.78	6.11	20	–13.8	R
10R-3, 89–	77.8	5.35	30	–19.5	R
10R-3, 92–	77.82	4.28	25	–78.4	R
10R-3, 94–	77.84	6.62	25	–39.4	R
10R-3, 96–	77.86	5.67	25	–35.9	R
10R-3, 98–	77.88	5.72	25	–43.1	R
10R-3, 100–	77.9	5.97	25	–39	R
10R-3, 102–	77.92	3.55	25	–42.2	R
10R-3, 104–	77.94	7.28	20	–26.9	R
10R-3, 106–	77.96	5.02	20	–12.5	R
10R-3, 108–	77.98	7.53	20	–8.3	R
10R-3, 110–	78	7.67	20	0.9	R?
10R-3, 112–	78.02	6.7	20	-15.4	R
10R-3, 114–	78.04	2.99	30	–35.4	R
10R-3, 116–	78.06	3.52	25	–41.2	R
10R-3, 118–	78.1	3.24	25	–79.1	R
10R-3, 120–	78.12	2.46	25	–69.4	R
10R-3, 122–	78.14	4.13	25	–30.8	R
10R-3, 124–	78.16	4.86	25	–27.6	R
10R-3, 126–	78.18	4.39	20	20.3	N
10R-3, 128–	78.2	3.26	20	20.9	N
10R-3, 130–	78.22	6.42	35	33.4	N
10R-3, 132–	78.24	5.24	20	-38.7	R
10R-3, 134–	78.26	6.84	20	–57.6	R
10R-3, 136–	78.28	6.93	20	–48.7	R
10R-3, 138–	78.3	3.13	20	–33.9	R
10R-3, 140–	78.32	1.22	25	–24.2	R
10R-3, 142–	78.34	2.4	34	–2.4	R
10R-3, 144–	78.36	3.54	34	4.4	N
10R-3, 146–	78.38	2.61	25	19.5	N
10R-3, 148–	78.38	4.7	25	24	N
10R-4, 7–9	78.67	3.82	70	66.9	N
10R-4, 59–61	79.19	4.82	70	–49.6	R
10R-4, 139–141	79.99	3	70	–76.1	R
10R-5, 4–6	80.14	13	70	–28.1	R
11R-1, 14–16	83.84	16.2	80	–48.1	R
11R-1, 52–54	84.22	4.48	80	18.6	N
11R-1, 65–67	84.35	7.99	80	–31.5	R
11R-2, 79–81	85.99	11.1	80	–68.1	R
11R-2, 98–100	86.18	10.4	80	–60.3	R
11R-3, 40–42	87.1	11	80	60.6	N
11R-3, 75–77	87.45	6.93	95	32	N
11R-4, 10–12	88.3	5.9	80	–51.6	R
11R-4, 110–112	89.3	13.2	80	38.6	N
11R-5, 2–4	89.72	7	80	35	N
11R-5, 29–31	89.99	30.8	80	66.7	N
12R-1, 71–73	94.11	12.8	99	–49.6	R
12R-1, 127–129	94.67	9.94	50	–56.8	R
12R-2, 32–34	95.22	8.86	75	51.4	N
12R-2, 70–72	95.6	7.04	80	38.7	N
12R-3, 69–71	97.09	11.1	70	–65.9	R
12R-3, 84–86	97.24	12.6	70	–43.4	R
14R-1, 15–17	112.85	19	80	–35.7	R
14R-1, 110–112	113.8	28.4	80	15	N
14R-1, 133–135	114.03	18.7	80	46.8	N
14R-2, 39–41	114.59	4.41	70	15.6	N
14R-2, 87–89	115.07	5.49	80	–56.1	R
14R-2, 126–128	115.46	13.6	80	42.6	N
14R-3, 13–15	115.83	14.4	80	66.9	N
14R-3, 89–91	116.59	16.3	99	–43.2	R
14R-3, 126–128	116.96	6.91	80	–51.8	R
14R-4, 24–26	117.44	5.09	80	–65	R
14R-4, 67–69	117.87	10.3	70	–61.1	R
14R-4, 91–93	118.11	8.31	80	–48.7	R
14R-5, 32–34	119.02	19.6	90	–55.1	R
14R-5, 107–109	119.77	19.4	80	–48.6	R
14R-5, 119–121	119.89	13.1	80	–59.2	R
14R-6, 14–16	120.34	8.87	70	–20.2	R
14R-6, 92–94	121.12	5.77	70	–24.7	R
14R-6, 140–142	121.6	1.7	80	–12.7	R
14R-7, 19–21	121.89	1.12	80	55.9	N
15R-1, 113–115	123.53	15.2	80	27.2	N
15R-1, 128–130	123.68	6.72	80	53.1	N
15R-2, 26–28	124.16	8.98	80	25.8	N
15R-2, 87–89	124.77	4.62	70	–66	R
15R-2, 128–130	125.18	8.31	99	–42.7	R
15R-3, 56–58	125.96	7.06	90	–53.5	R
15R-3, 65–67	126.05	8.08	90	–61.3	R
15R-3, 137–139	126.77	3.12	80	74.5	N
15R-4, 25–27	127.15	8.8	60	–62.6	R
16R-1, 33–35	132.33	0.05	20	42.4	N
16R-1, 72–74	132.72	5.97	70	–14.2	R
16R-2, 79–81	134.29	0.05	30	55.7	N
16R-2, 115–117	134.65	4.26	80	50.5	N
16R-3, 38–40	135.38	0.06	40	43.3	N
16R-3, 120–122	136.2	0.19	60	–15.7	R
16R-4, 14–16	136.64	0.87	95	–18.9	R
16R-4, 76–78	137.26	3.83	60	–45.7	R
16R-5, 27–29	138.27	11.7	60	38.6	N
16R-5, 39–41	138.39	2.02	80	46.3	N
16R-6, 42–44	139.92	7.53	80	34.2	N
16R-6, 101–103	140.51	0.19	55	41.7	N
17R-1, 25–27	141.85	2.41	80	–42.3	R
17R-1, 107–109	142.67	2.39	40	–53.4	R
17R-2, 24–26	143.34	0.06	15	–21.9	R
17R-2, 37–39	143.47	4.52	70	–40R	
17R-3, 20–22	144.8	4.43	90	–64.2	R
17R-3, 36–38	144.96	0.09	15	80	N?

Note: See Table 1 for explanation of abbreviations.

Table 6. Paleomagnetic and biostratigraphic datums at Hole 900A.

Magnetic datum (Chron or subchron)	Biostratigraphic datums (N, F)	Age (Ma) (magnetism)	Age (Ma) (biostratigraphy)	Depth range (mbsf) (magnetism)	Depth range (mbsf) (biostratigraphy)
Jaramillo	NN19f	0.99–1.07	0.89–1.06	21.08	21.76–26.62
Olduvai	NN19a, N23/N22	1.77–1.95	1.66–1.91	47.00–48.06	43.86–47.96
Matuyama/Gauss	NN16	2.58		64.55	64.95–79.29
Mammoth		3.22–3.33		76.9–78.7	
Gauss/Gilbert	NN15, N19	3.58		79.19	84.42–89.39
Cochiti		4.18–4.29		84.2–84.4	
Nunivak		4.48–4.62		87.1–87.5	
Sidutjall		4.8–4.89		89.3–90.0	
Thvera		4.98–5.23		95.2–95.6	
C3An,1n		5.83–6.05		113.8–114.6	
C3An, 2n		6.17–6.45		115.4–115.8	
C3Bn		6.79–6.94		121.9–124.2	
C3Br, 1n		6.98–7.02		126.8–127.2	
C3Br, 2n		7.18–7.22		132.3–132.7	
C4n, 1n		7.27–7.4		134.3–136.2	
C4n, 2n		7.48–7.9		138.3–140.5	
C4r, 1n		8.06–8.09		144.9–?	

Notes: N = nannofossil, F = foraminiferal datums.

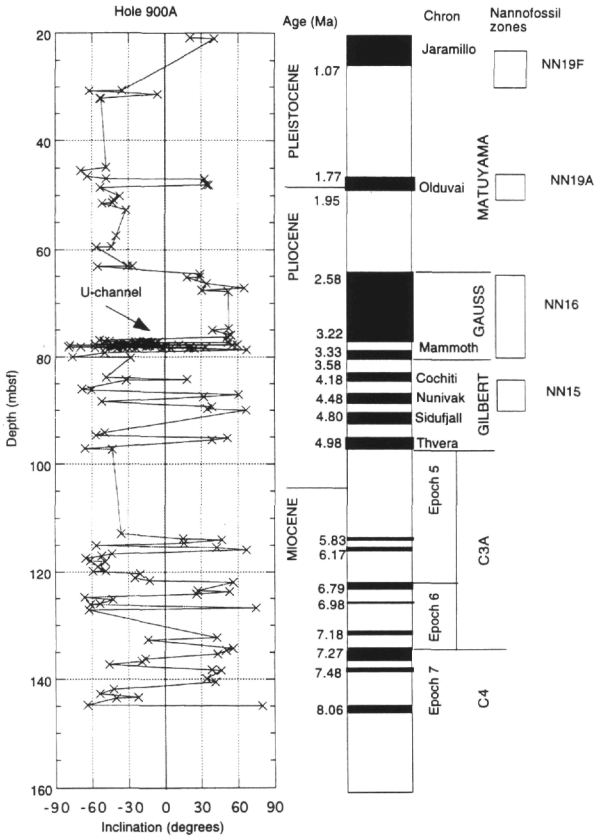

Figure 13. Downhole variation of stable magnetic inclination, inferred polarity, and biostratigraphic zones for Cenozoic sediments at Site 900. Normal polarity is indicated by black areas; reversed polarity is indicated by white areas.

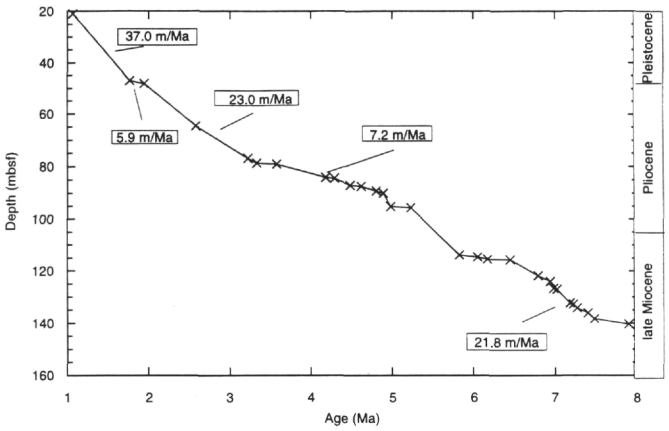

Figure 14. Depth vs. age curve for Hole 900A. The paleomagnetic data points are listed in Table 6. Two sedimentary hiatuses are inferred in this plot: one is close to the Pliocene-Pleistocene boundary, in an identical position to that proposed at Sites 897 and 898, and the other is in the interval of 3.58- 4.89 Ma at about 85 mbsf, which is close the Pliocene-Miocene boundary. It is important to note the absence of direct paleontological evidence for these hiatuses.

Table 7. Results of reversal tests using inclination only statistics.

Site	P	N	I	a95	k	R	μo	μc
897	N	23	41.17	6.04	23.85	22.0774		
	R	39	50.5	5.78	16.65	36.7181		
	M	62	47.02	4.58	17.0	58.4128	13.5	8.85
898	N	13	46.95	8.75	22.6	12.4668		
	R	73	45.33	4.91	13.35	67.6047		
	M	86	45.58	4.39	14.34	80.0712	1.2	11.6
900	N	5	32.8	11.6	59.65	4.9329		
	R	9	49.1	18.3	9.05	8.1163		
	M	14	43.1	12.3	10.9	12.8093	22.68	24.18

Notes: P = polarity; N (within polarity column) = normal; R = reversed; M = both N and R. N (table heading) = number of samples exhibiting the ChRM inclinations and used in statistical analysis; I = estimated mean inclination using the method of McFadden and Reid (1982); a95 = radius of circle of 95% confidence about the mean inclination in degrees; k = Fisher (1953) precision parameter for the mean inclination; R = length of resultant vector; μo/μc = observed/critical (at the 95% confidence level) angles between the normal and reversed mean inclinations (McFadden and McElhinny, 1990). If μo > μc, then the hypothesis of a common mean direction may be rejected at the 95% confidence level, or the reversal test is considered to be positive.